THE MEASUREMENT OF ISOMERIC CROSS-SECTION RATIOS IN NEUTRON INDUCED REACTIONS

By

NAWAL SHAFIG SHAKIR

A thesis submitted for the degree of

Master of Philosophy

Department of Physics
The University of Aston in Birmingham

June 1978

THE MEASUREMENT OF ISOMERIC CROSS-SECTION RATIOS IN NEUTRON INDUCED REACTIONS

A thesis submitted for the degree of M.Phil in the University of Aston in Birmingham, June 1978.

by

NAWAL SHAFIG SHAKIR

SUMMARY

A method of measuring the isomeric cross-section ratios of nuclear reactions is described and discussed. This method relies on an analysis of the time behaviour of the decay of the ground state. Since only the ground state activity is observed many of the sources of error present in methods which rely on measuring the activities of the ground state and isomeric state separately are avoided.

Results are given for measurements of the isomeric cross-section ratios for the reaction $^{45}Sc(n,2n)^{44}Sc$ at incident neutron energies of 13·1, 14·4 and 15·4 MeV and for the reaction $^{115}In(n,2n)^{114}In$ at incident neutron energies of 13·2, 14·1 and 14·9 MeV. These results are compared with those of other workers.

The reactions $^{198}Pt(n,2n)^{197}Pt$ and $^{76}Ge(n,2n)^{75}Ge$ are also discussed briefly. For the former results obtained by measuring the two states separately are given.

A discussion of theoretical factors affecting isomeric cross-section ratios is given.

Key words: Nuclear Reactions

Cross-sections

Isomeric Ratios

ACKNOWLEDGEMENTS

I am greatly indebted to my supervisor Dr. P.E. Francois for his help and consideration at all times, but especially during the latter part of this work. My thanks are also due to H.E. Biggs and J. Phull for carrying out the bombardments needed.

Finally I would like to thank Mrs. L. Francois for her efficient typing of this thesis.

An International Atomic Energy Agency Fellowship provided financial support for most of the time I was engaged upon this work.

PREFACE

This thesis describes a method of measuring the isomeric cross-section ratios of nuclear reactions. This method relies on an analysis of the time behaviour of the decay of the ground state.

Calculation for optimum time of irradiation together with the effect of change of flux during the irradiation on the isomeric ratio was discussed.

The results of isomeric cross-section ratios for the reactions $^{45}Sc(n,2n)^{44}Sc$ and $^{113}In(n,2n)^{112}In$ at different neutron energies are given.

The reactions $^{198}Pt(n,2n)^{197}Pt$ and $^{76}Ge(n,2n)^{75}Ge$ are also discussed briefly.

The way in which the statistical model and evaporation theory may be used to analyse the production of isomers is given briefly.

CONTENTS

CONTENTS (contd)

CONTENTS (contd)

CHAPTER I

INTRODUCTION

I.1 Explanation of isomeric states. Conditions for their existence.

Some radioactive nuclides have nucleon combinations that are stable with respect to alpha or beta decay, yet have an excess of internal energy. This excess energy may be released in several ways, the most common of which is the emission of electromagnetic radiation (photons) with discrete quanta of energy. These radiations are called gamma rays. If the de-excitation takes place within a life time that is easily measured, such radioactive nuclides are known as metastable isotopes and the transition is considered a radioactive decay process called an isomeric transition (IT). The designation for a metastable nuclide is by adding an m after the mass number; for example, the metastable state of ^{60}Co is ^{60m}Co.

The other common way for a nucleus to lose excess energy is by an electromagnetic interaction between the nucleus and orbital electrons which results in the emission of an electron whose kinetic energy is equal to the nuclear transition energy, less the binding energy of the emitted electron. This process called internal conversion (IC) competes with γ-ray emission as a de-excitation process.

The existence of an isomeric transition results in a pair of nuclei that have the same mass number and atomic number, but one has more energy than the other, and, therefore, has different radioactive and other properties. A pair of such nuclei are nuclear isomers and the phenomenon

is nuclear isomerism.

There are two factors that are primarily responsible for a very low transition probability of gamma emission:

a. A large difference in the total angular momentum, (I), between the excited state and the lower excited state or the ground state.

b. A small energy difference between the two states.

The reason for the small transition probability and long half-life for the isomeric state can be explained with the help of a single-particle model[1] for odd A nuclides. As a shell approches closure, the single particle levels lie very close, and therefore the transition will have very small energies. Usually a level from the higher oscillator states falls down to the lower oscillator level near the closure of a shell. This combination of high spin difference and low energies makes the transition very slow.

I.2 Explanation of cross-section and definition of isomeric ratio

When a neutron collides with a nucleus three important types of interactions can occur: elastic scattering, inelastic scattering, and nuclear reactions. In all of these cases the total charge is constant, there is conservation of total energy, and of total momentum. If the scattering is elastic, the kinetic energy is divided between the neutron and the nucleus. In fact it can be considered as an (n,n) reaction. In the inelastic scattering the nucleus is left in an excited state and the reaction is represented by an (n,n') reaction. In nuclear reactions the neutron is captured forming a compound nucleus which emits photons in the case of radioactive capture or

elementary particles, e.g. a proton, α-particle, and in some cases fission occurs.

In Table 1[2] the most frequently occurring reactions are shown as a function of neutron energy. The reactions are given in decreasing order probability although there are exceptions.

The probability of a nuclear reaction occurring is expressed by the cross section, σ. For a thin foil placed in a neutron beam one defines[2]:

$$\sigma = \frac{\text{number of events of a certain type per second per nucleus}}{\text{number of neutrons incident per cm}^2 \text{ per second}}$$

$$= \frac{\text{reaction rate}}{\text{neutron flux}} \quad \text{in cm}^2$$

Most cross-sections are of the order of 10^{-24} cm^2, it has become convenient to express cross-sections in the units of the barn, where

$$1 \text{ barn} = 10^{-24} \text{ cm}^2$$

Where several types of events are possible as already mentioned before, each has a certain probability of occurring and, thus, cross-section. The total cross-section σ_T can be considered as a sum of σ_s and σ_a :

$$\sigma_T = \sigma_s + \sigma_a$$

where $\sigma_s = \sigma(n,n) + \sigma(n,n')$

$$\sigma_a = \sigma(n,2n) + \sigma(n,p) + \sigma(n,d) + \sigma(n,\gamma) + \cdots$$

At 14MeV the probability of a (n,γ) reaction is quite small though not always negligible. The most important reactions are due to (n,2n), (n,p), and (n,α). The bombarding neutrons may have an interaction probability for forming the isomeric states of the daughter nucleus.

The isomeric cross-section ratio for a certain reaction is defined as the ratio of the cross-section,

TABLE 1

Interaction of neutrons with nuclei

Neutron energy	Nuclear reactions with nuclei	
	$25 \leqslant A < 80$	$80 \leqslant A < 240$
0 - 1 KeV	(n,n) (n,γ)	(n,γ) (n,n)
1 - 500 KeV	(n,n) (n,γ)	(n,n) (n,γ)
0·5 - 10 MeV	(n,n) (n,n') (n,p) (n,α)	(n,n) (n,n') (n,p) (n,γ)
10 - 50 MeV	(n,2n) (n,n') (n,n) (n,p) (n,np) (n,2p) (n,α)	(n,2n) (n,n') (n,n) (n,p) (n,np) (n,2p) (n,α)

σ_m, of a reaction producing the residual nucleus in a metastable state to the cross-section, σ_g, of the reaction leaving the nucleus in the ground state.(3)

It is dependent on the distributions of angular momenta in various stages of the reaction. These distributions in turn depend on the mechanism of the reaction.

I.3 Importance of knowledge of isomeric ratios

The measurement of the isomeric cross-section ratio is important from a number of points of view. It can be used to study both the transfer of angular momentum in nuclear reactions and the spin dependence of the nuclear level density in the final nucleus via the spin cut-off parameter.(4) Secondly neutron excited nuclear isomers may be useful for the measurement of neutron energy when used as threshold detectors.(5) Thirdly a knowledge of the isomeric ratio is also desirable if it is proposed to use the reaction for neutron activation analysis.

I.4 Methods of measuring the isomeric cross-section ratios

I.4.1 Many methods are based on measuring the cross-sections for isomeric state and ground state separately, relative to a monitor reaction(6), by irradiating the sample and monitor substance. Absolute activities of the isomeric state and the ground state have been measured, and used in calculating the individual cross-sections. The isomeric ratio was calculated from these cross-sections.(7,8,9)

I.4.2 Alternatively, the induced activities of the sample are measured, the decay curves of the isomeric transition and ground state are followed separately(10,11,12,13),

(separate irradiations of different periods being needed for studies of isomeric levels differing strongly in half-life).[14,15]

The cross-sections can be calculated and the isomeric ratio determined.

Some early methods were based on measuring the total activity, A(t), where

$$A(t) = A'e^{-\lambda gt} + A''e^{-\lambda mt}$$

The quantities A', activity of the ground state, and A'', activity of isomeric state, are computed by the least squares method.[3] From A' and A'' the cross-sections due to ground state and isomeric state can be calculated, and the isomeric ratio determined.

I.5 Outline of the present method

The samples were bombarded for a period of time depending on the half-lives of the nuclides under investigation. The irradiated sample was then placed on the selected detector, and the counts arising from ground state decay for different fixed time intervals were measured. By applying the method of least squares to the time behaviour of the decay of the ground state, the isomeric cross-section ratio can be determined.

This technique takes advantage of the fact that members of an isomeric pair are genetically related in that the ground state is populated both by direct (n,2n) reaction and by isomeric transition from the isomeric state.

As only the ground state activity is measured, the results so obtained are independent of several sensitive factors such as photopeak detection efficiency, γ-ray intensity, absorption corrections, determination of neutron

fluxes, and sample uniformity. These factors invariably constitute the major portion of the uncertainty in the results of earlier experiments.

This method was attempted for measuring the isomeric cross-section ratios for (n,2n) reactions on the isomeric pairs $^{44m,g}Sc$. $^{112m,g}In$, $^{197m,g}Pt$, and $^{75m,g}Ge$.

A similar approach has recently been reported by Kao and Alford.[16]

CHAPTER II

EXPERIMENTAL ARRANGEMENTS

II.1 Introduction

In principle, activation measurement is similar to other instrumental methods in that energy in some form is put into the material and the characteristic radiation emitted from the material is detected. In its simplest form, neutron activation requires a source of neutrons, a detector for the characteristic radiations emitted after irradiation, some means of transferring the sample between the neutron source and detector, instrumentation to select the correct radiation and analyze the data.

II.2 Source of neutrons

II.2.1 The high voltage generator and accelerator

The Van de Graaf generator[17] is shown diagrammatically in fig. 2.1. The spray combs consisted of eighty-eight sharp needles mounted in blocks of eight set 1/8'' from the rotating belt and level with the bottom pulley. The needles were supplied with a variable potential of 0 to 12 kV obtained from a conventional power pack. The sharp points caused ionization of the air and repelled the positive ions. These positive ions were collected by a rubberized canvas belt 10 inches wide which rotated at 3,000 ft. per min. The positive charges on the belt were collected by the collector points. These points conveyed the charge to the top terminal. By using another set of spray points that spray negative charge, the charge-carrying capacity of the belt is doubled. The charge collection process at the high-potential terminal may be continued indefinitely. A limit is reached when the

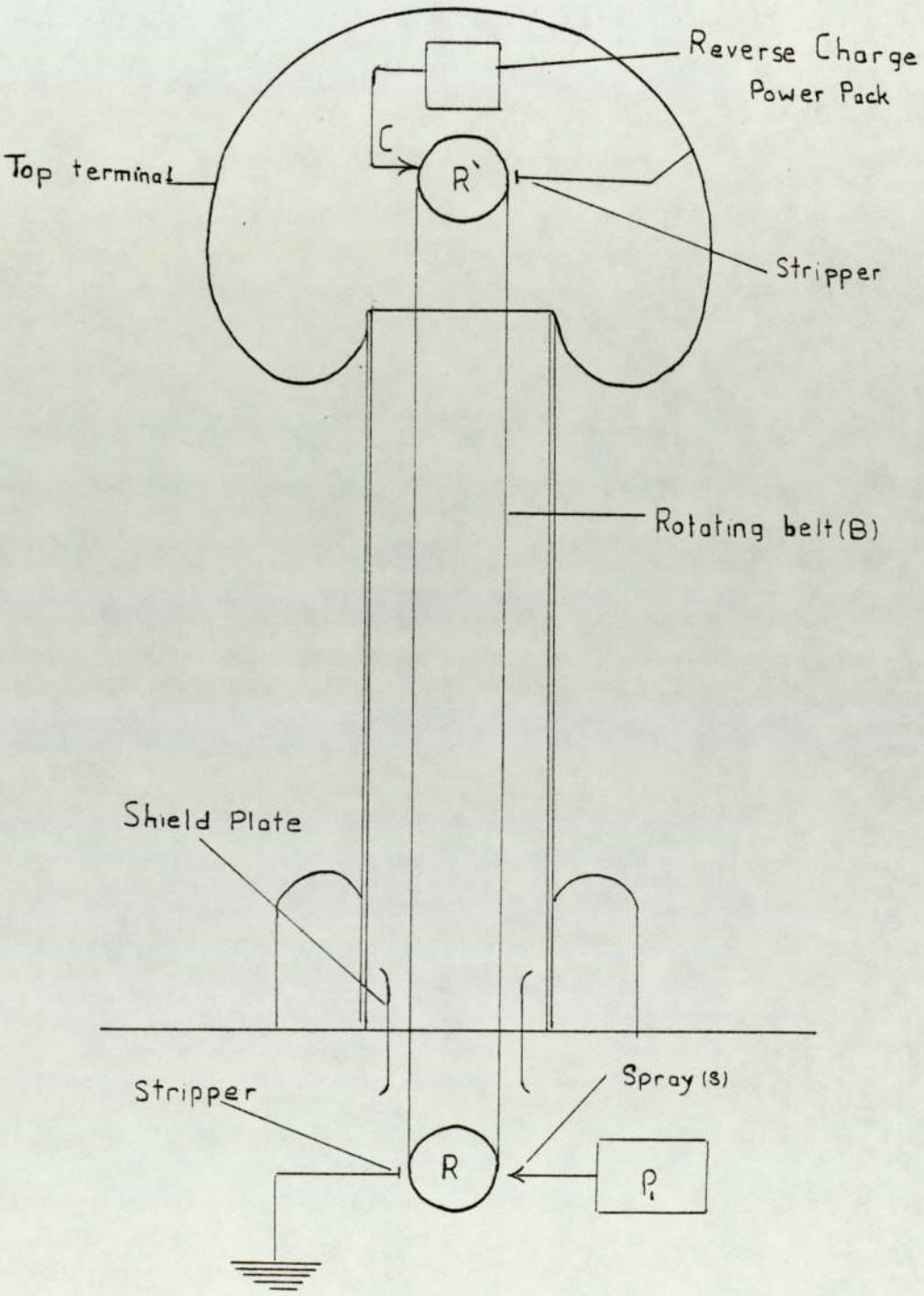

Fig 2.1 High voltage generator

insulation breaks down and the loss of charge by stray currents is equal to the charge transferred by the belt.

The generator was positioned next to the accelerator tube and the top terminals linked by a brass strip. The power motor was located underneath a steel platform and the belt ran through a hole in the floor which was fitted with earthed shield plates to prevent loss of charge from the belt. The motor and bottom pulley were enclosed in a box inside which heaters were situated to prevent the belt from becoming damp.

The porcelain accelerator tube[18] consisted of three cylindrical sections 44 cm long with an internal diameter 25·4 cm and external diameter of 30 cm. Inside each section seven stainless steel bands, sprung against the surface of the porcelain, supported seven spun aluminium electrodes. These electrodes protected the walls of the accelerator tube from the ion beam which passed through a 19 cm diameter hole in the centre of the electrodes. Fig. 2.2 shows schematically one section of the accelerator tube. The electrodes were connected externally, through vacuum seals, to a resistance chain of 10^{11} ohms, which acted as a potential divider and provided a constant potential gradient down to the accelerator tube. The focussing ability of a lens system is determined by the ratio of the potential difference across the lens to the energy of the ion passing through the lens. This ratio implies, therefore, that the lens located at the beginning of the accelerator tube possessed stronger focussing action than the lens situated at the end of the tube.

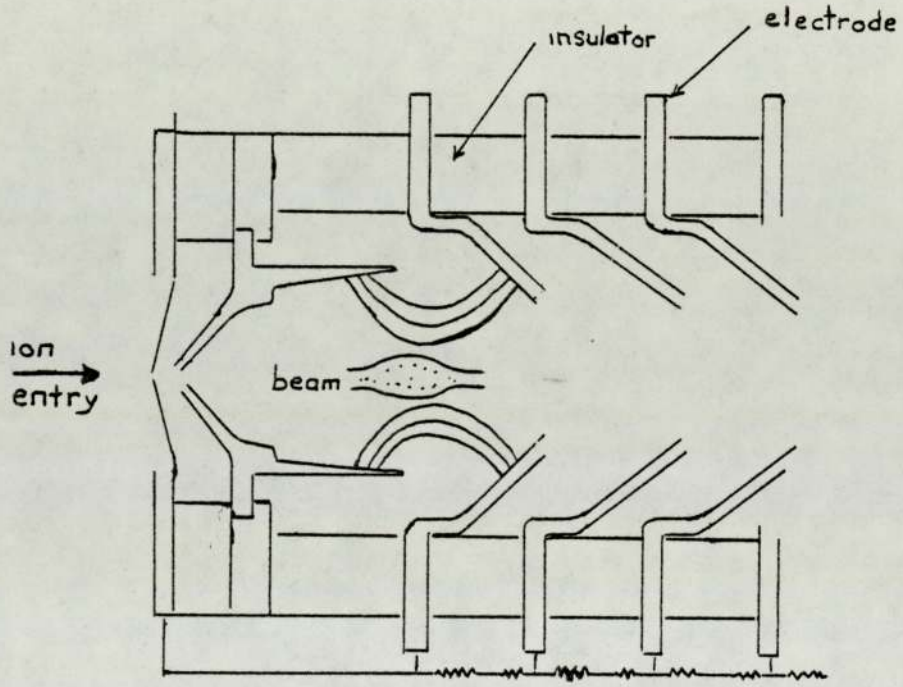

Fig (2.2) Van de Graaff accelerating tube

On top of the accelerator tube, in the domed top terminal were the ion source[19] and gas leak, which controlled the gas supply to the ion source in a steady and reproducible manner, together with the oscillator, extractor and the beam focus controls.

II.2.2 Targets

The thick target used for the production of neutrons, (shown in fig. 2.3), was obtained from the Radiochemical Centre, Amersham, and consisted of a copper base 28·6 mm diameter and 0.05 cm thick onto which a layer of titanium 1·09 mg/cm^2 was deposited. An active area of 25·4 mm diameter was formed by absorbing 4 curies per cm^2 of tritium onto the surface.

Such targets are prepared as follows: the titanium is evaporated on copper as a backing material and then exposed to an atmosphere of tritium to form the inter-metallic compound, titanium tritide. Such targets are very productive and with good cooling can stand high ion currents. The tritium absorbed onto the surface has a half-life of 12 years and emits β^- radiation. The life-time of a tritium target is determined by displacement of tritium atoms in the target by deuterium atoms in the beam. Target performance is degraded if the vacuum system is not clean and a deposit of carbonaceous material forms on the surface which reduces the deuteron energy before the deuterons can reach the tritium. Thick tritium titanium target mounted on the target assembly is shown in fig. 2.4.

The target was isolated electrically from the beam tube itself and operated at few hundred volts positive relative to the beam tube, which was grounded. This

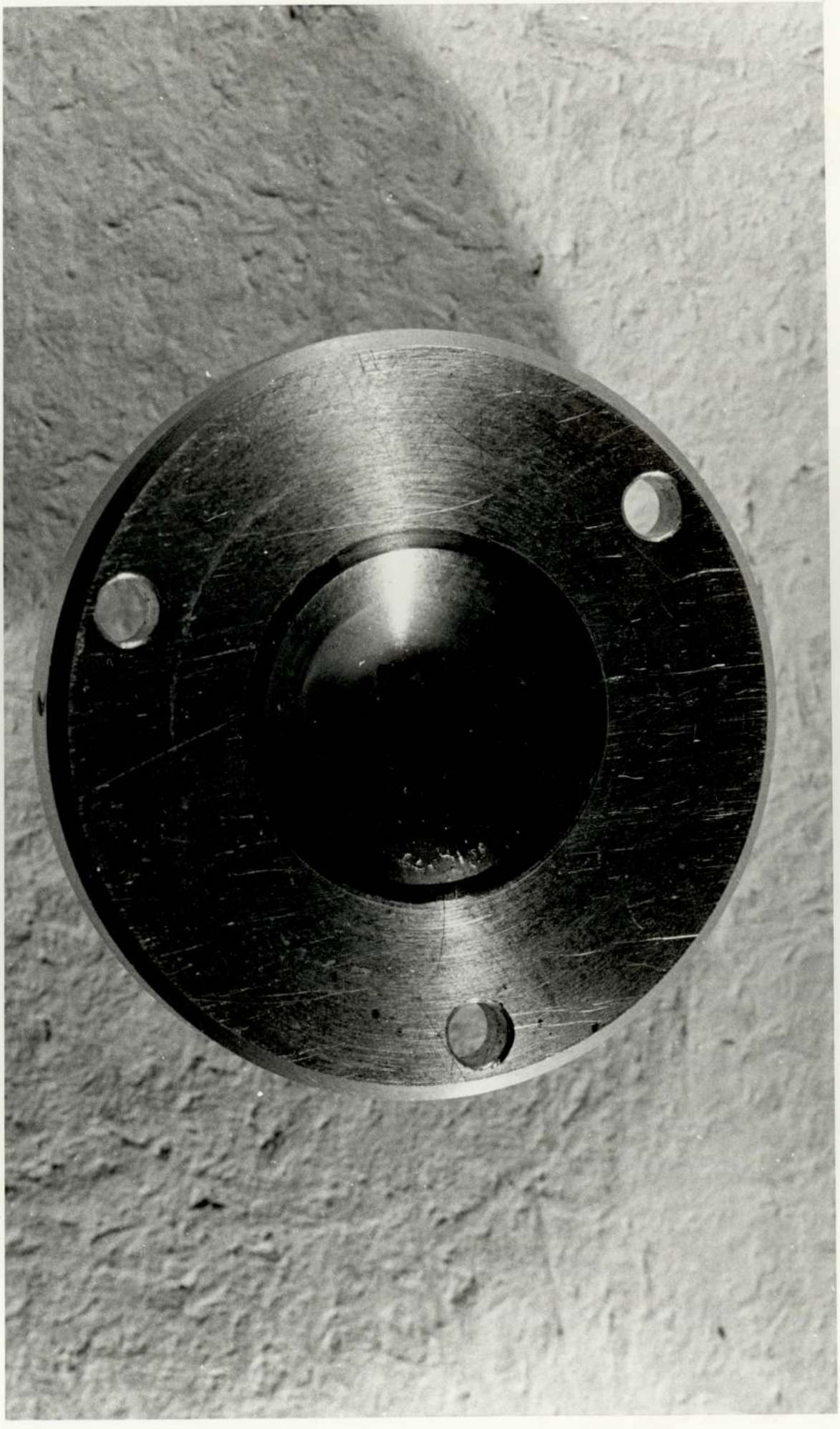

Fig 2.3

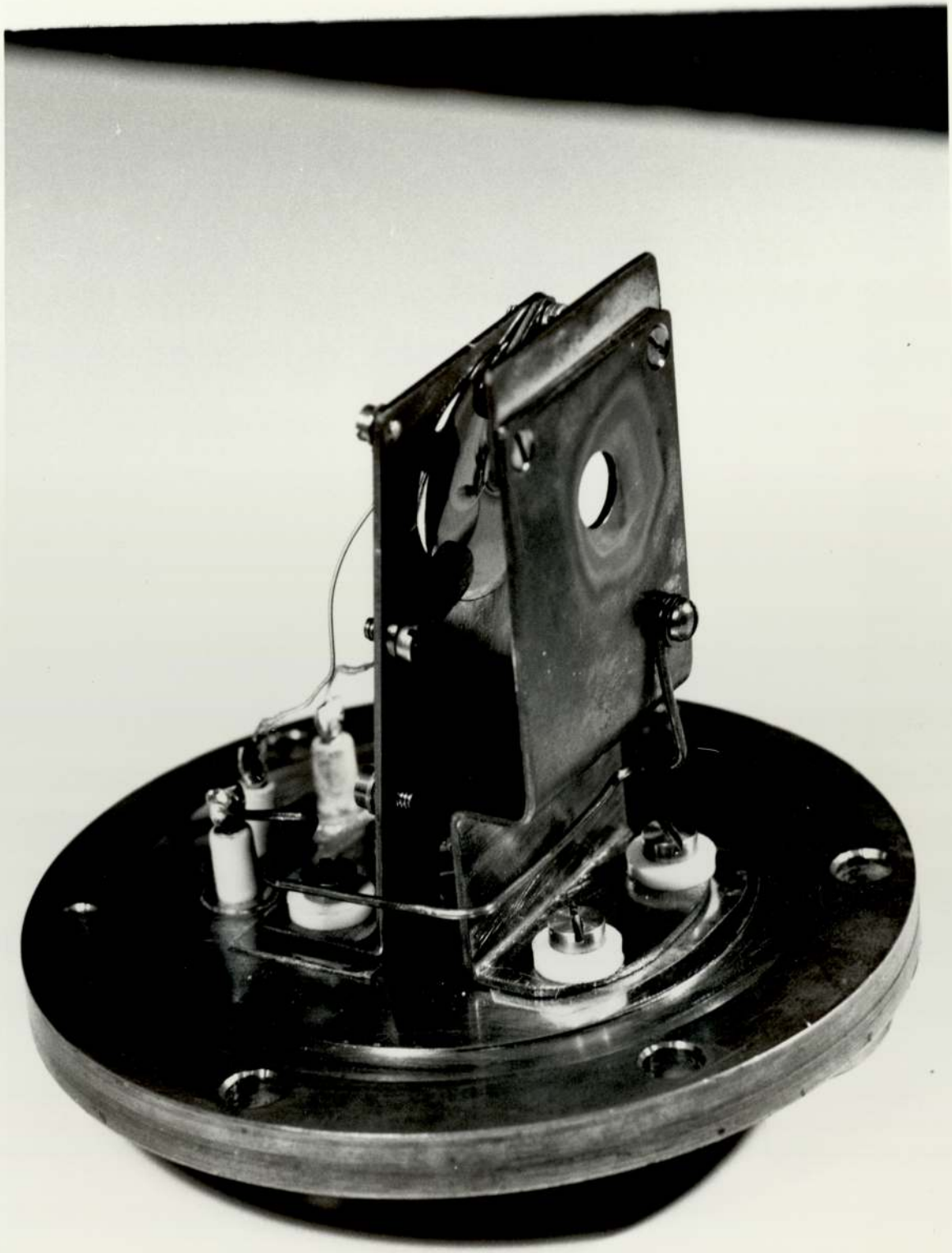

Fig 2.4

provided a voltage for suppression of secondary electrons generated in the target when the ion beam struck it. Without this suppression, a beam of secondary electrons would be accelerated back up the accelerating structure, which would produce an additional load on the high voltage power supply.

The control system for the accelerator, fig. 2.5, was mounted in a separate room to isolate the control function from the high radiation area near the accelerator. Controls were provided here to control the accelerating voltage, beam current, beam focus, and switching off the various sub-systems. The control room also contained two interlocks to shut down the accelerator if any of the operating parameters are outside a safe range for the accelerator.

II.2.3 Production of neutrons

Neutrons of approximately 14 MeV produced by the reaction of deuterium and tritium, which can be expressed as

$$^{2}H + {}^{3}H \longrightarrow {}^{4}He + n + 17{\cdot}586 \text{ MeV} \qquad \text{(II.2.1)}$$

This reaction is a prolific source of high-energy neutrons, as can be seen from the excitation function[20] illustrated in fig. 2.6.

The dependence of the emergent neutron energy as a function of laboratory angle, fig. 2.7, was condensed from the information of Fowler and Brolley[21]. The relative small spread of the neutron energy through large changes in the laboratory angle may be noted, it was used to estimate energy spread on samples. For example, the difference between the neutron energy at 150° and that at

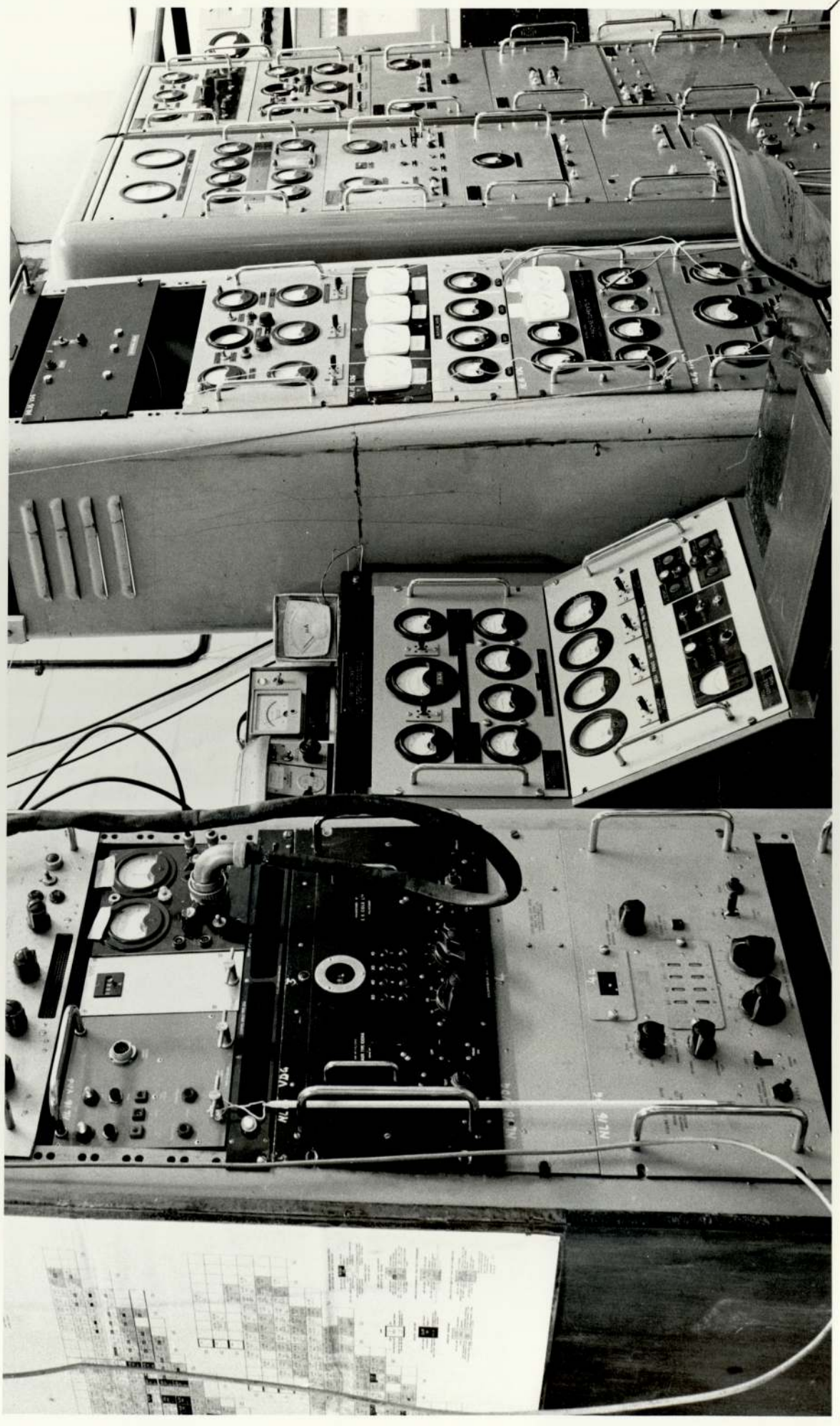

Fig 2.5

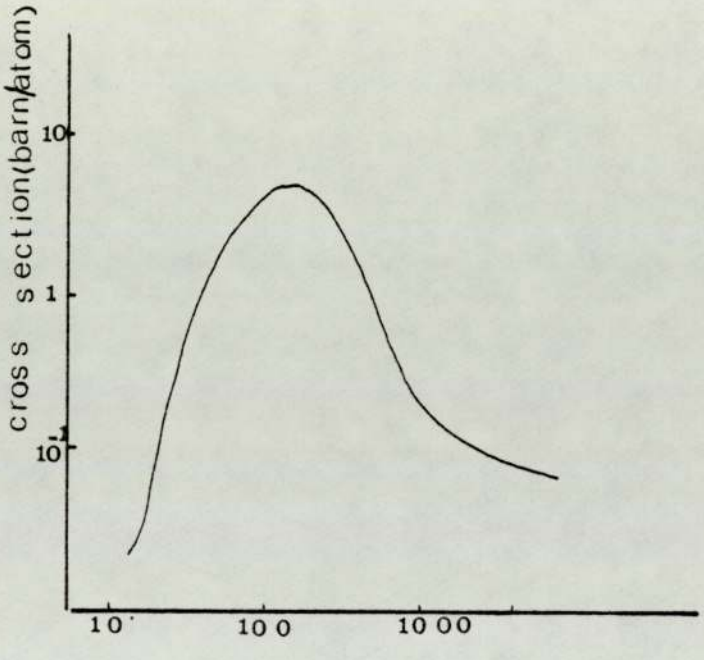

Fig (2.6) excitation function

for the D-T reaction

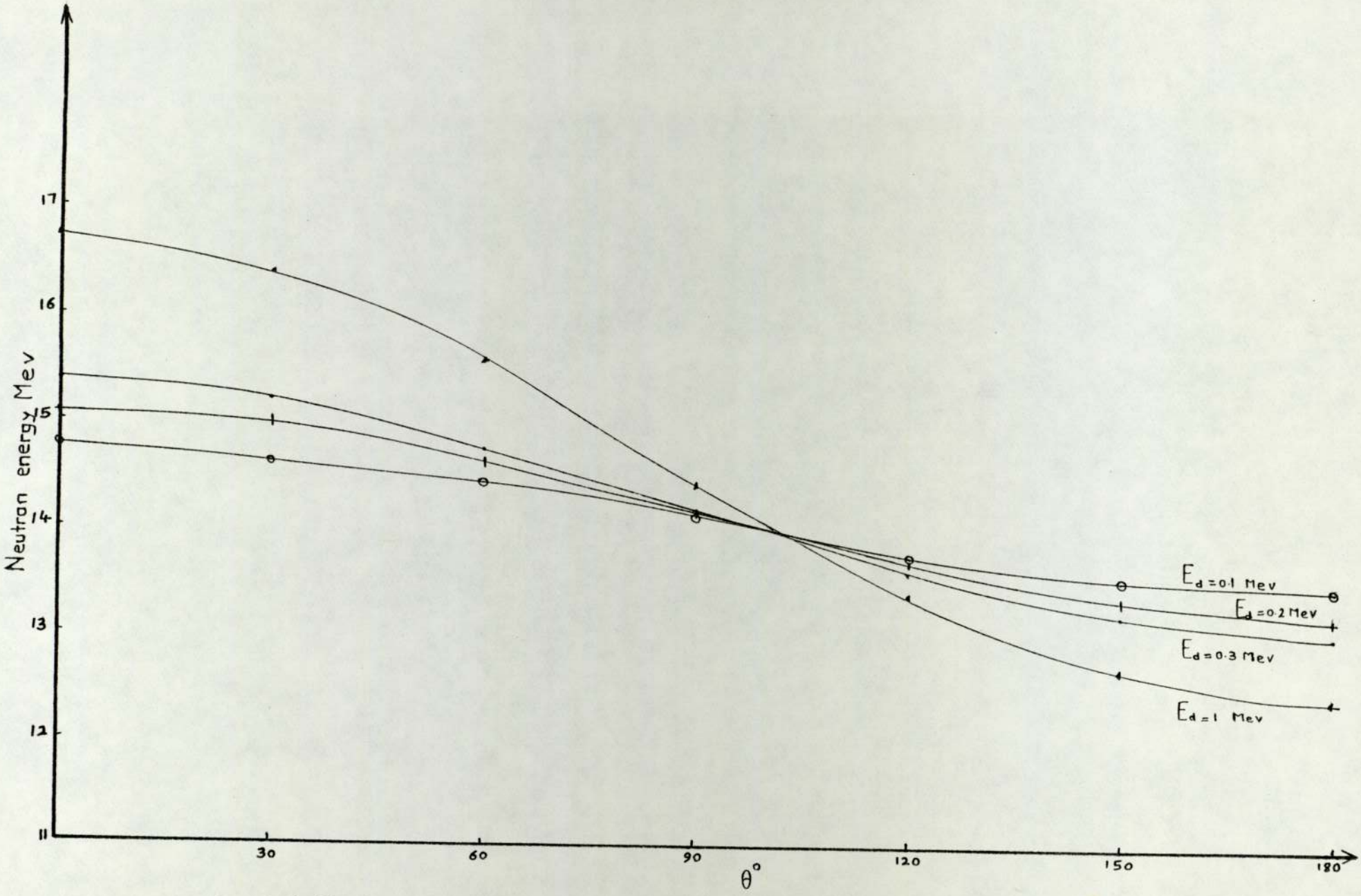

Fig 2.7 Neutron energy as a function of laboratory angle θ°. E_d is the energy of the incident deuteron (D - T) reaction.

0° is only about 2·2 MeV for incident deuterons energy of 300 KeV. An interesting observation to be made from an examination of fig. 2.7 is that, at an angle of about 100°, the neutron energy remains essentially constant at a value of about 14 MeV and is independent of acceleration voltage of about 500 KeV. Therefore, a sample placed at an angle of 100° would experience a neutron flux whose energy is independent of the bombarding deuteron energy within the accelerating limit of the neutron generator.

For thick targets(thin or thick is a function of incident deuteron energy) Burrill[22] gives the neutron yield as illustrated in fig. 2.8, the neutron yield can be calculated from an integral of the target stopping power and the D-T reaction cross-section. The effect of target thickness on the neutron intensity is clearly explained. Experiments have proved that thick target fluxes closely approximate to isotropy.

II.3 Rapid transfer system

In the case of very short half-life nuclides, some kind of rapid transfer mechanism must be used to move the sample to the neutron generator for irradiation and back to the detector for counting. For the present experiments a system was set up in which the sample is introduced at the sending station. Air pressure is applied from a blower by a switch to transport the sample to the irradiation site, the sample was stopped inside a cadmium covered plastic tube, directly in front of the neutron generator target. After irradiation the sample was released by reversing the switch and transferred in a few seconds through a plastic tube about 50 m length to the counting room.

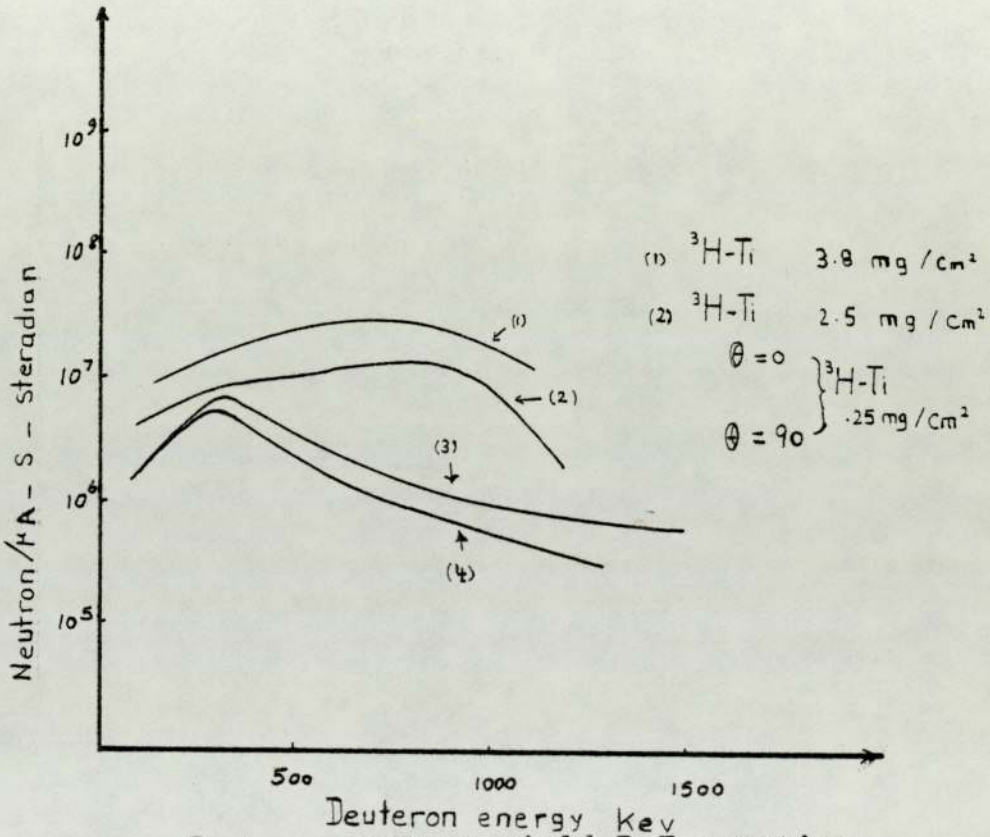

Fig (2.8) neutron yield D-T reaction

II.4 Detection

Once the sample has been irradiated, it is then necessary to characterize and measure the nature of the resulting radiation by the process of detection. There are a number of detection devices available for radiation measurement. These include the two types which were used in this work, the scintillation counters, and semiconductor detectors.

Before the operation and characteristics of these two devices are explained, one has to discuss the interaction of γ-rays with detectors.

II.4.1 Interaction of γ-rays with the detector

Gamma rays interact with matter in three significant ways,(23)

1. Photoelectric effect.

This is an absorption process in which a γ-ray, energy $E_\gamma = h\nu$, ejects an electron, with energy E_e, from an atomic orbit and disappears by transferring all its energy in the process. Thus

$$E_e = h\nu - \beta_e \qquad \text{(II.4.1)}$$

β_e is the binding energy of the electron. The atomic absorption coefficient of the photoelectric effect, μ_{pe}, is given by

$$\mu_{pe} \propto Z^5 E_\gamma^{-3.5} \ \text{cm}^2/\text{atom} \qquad \text{(II.4.2)}$$

where

Z atomic number of the absorbing material.

It is clear that the photoelectric absorption is more important for lower γ-rays in the heavier elements.

2. Compton effect

This is an inelastic scattering process in which the photon, $E_\gamma = h\nu$, ejects an electron, E_e, but escapes with degraded energy, $E_\gamma^1 = h\nu^1$, making an angle ϕ with the direction of the first photon given by

$$E_\gamma^1 = \frac{E_\gamma}{1 + \frac{E_\gamma(1 - \cos \phi)}{mc^2}} \qquad (II.4.3)$$

E_e reaches its maximum value when $\phi = 180$ and

$$E_{emax} = \frac{E_\gamma}{1 + \frac{mc^2}{2E_\gamma}} \qquad (II.4.4)$$

The atomic absorption coefficient, μ_c, is given by

$$\mu_c \propto \frac{Z}{E_\gamma} \left(\ln \frac{2E_\gamma}{mc^2} + \frac{1}{2}\right) \qquad (II.4.5)$$

3. Pair production

This is an absorption process in which the photon, (with energy $E_\gamma > 2m_e c^2$ MeV) vanishes in creating a positively and negatively charged pair of electrons, with total kinetic energy, E

$$E = E_\gamma - 1{\cdot}02 \text{ MeV} \qquad (II.4.6)$$

The atomic absorption coefficient, μ_{pp}, at energies just above 1·02 MeV is given by

$$\mu_{pp} \propto Z^2 (E_\gamma - 2mc^2) \qquad (II.4.7)$$

At high energies the dependence becomes logarithmic

$$\mu_{pp} \propto Z^2 \log (E_\gamma) \qquad (II.4.8)$$

Pair production was not involved in the present work, because none of the γ-rays observed had an energy above 1·02 MeV.

II.4.2 The NaI(Tl) scintillation detector

Scintillation detectors or phosphors of many types are available for many applications. The phosphors include

organic solids, organic phosphors in plastic solids, organic solutions, inorganic solids and inorganic gases. The luminescence of inorganic solids such as NaI(Tl) is primarily due to the presence of an activator. A gamma photon interacts with the crystal resulting in the production of high energy electrons. These electrons are slowed down and lose their energy principally to electrons of the crystal. This results in excitation and ionization of the crystal constituents. The energy deposited in the crystal then migrates to an activator or luminescent centre, from which a transition to the ground state occurs by the emission of a light photon. NaI crystals activated with thallium were used in this work. The presence of activators in the crystals produces local energy levels (centres) in the forbidden region of the energy band diagram, below the conduction band. By absorption of γ-rays an impurity centre may be raised to the excited state, the absorption process can be represented by the transition A - B in fig. 2.9, migrating to position C by thermal dissipation of the excess energy. The luminescent photon is emitted as transition C - D, following which the centre returns to minimum energy in the ground state by further thermal dissipation of excess energy.

The luminescence emitted by the crystal following excitation by the absorbed radiation follows an exponential decay with time

$$I = I_o \; e^{-t/\tau} \qquad \text{(II.4.9)}$$

where τ is the decay time ($\approx$ 0·25 μsec.)
This light interacts with the photocathode of a photo-multiplier and ejects electrons. Figs 2.10, 2.11. These electrons were multiplied so that a very large resultant shower of

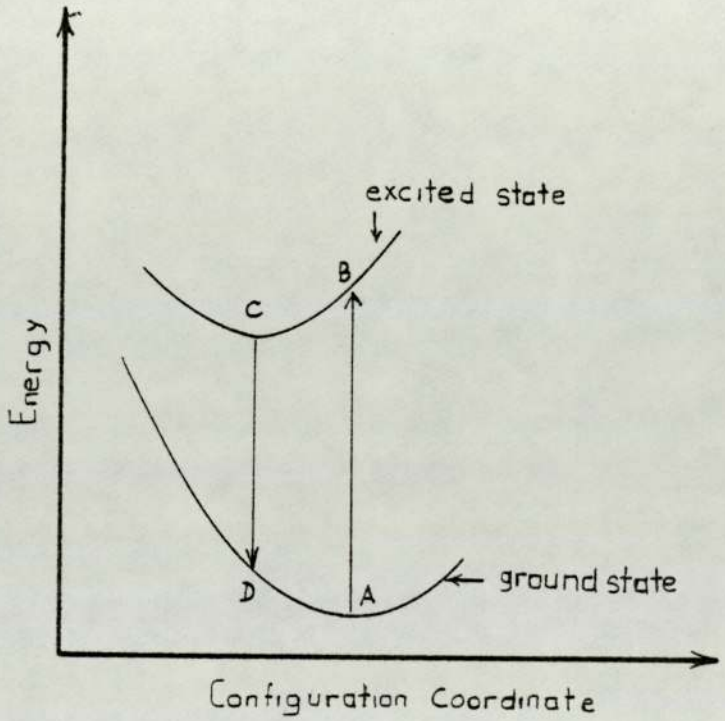

Fig 2.9 Potential energy levels of an activator centre

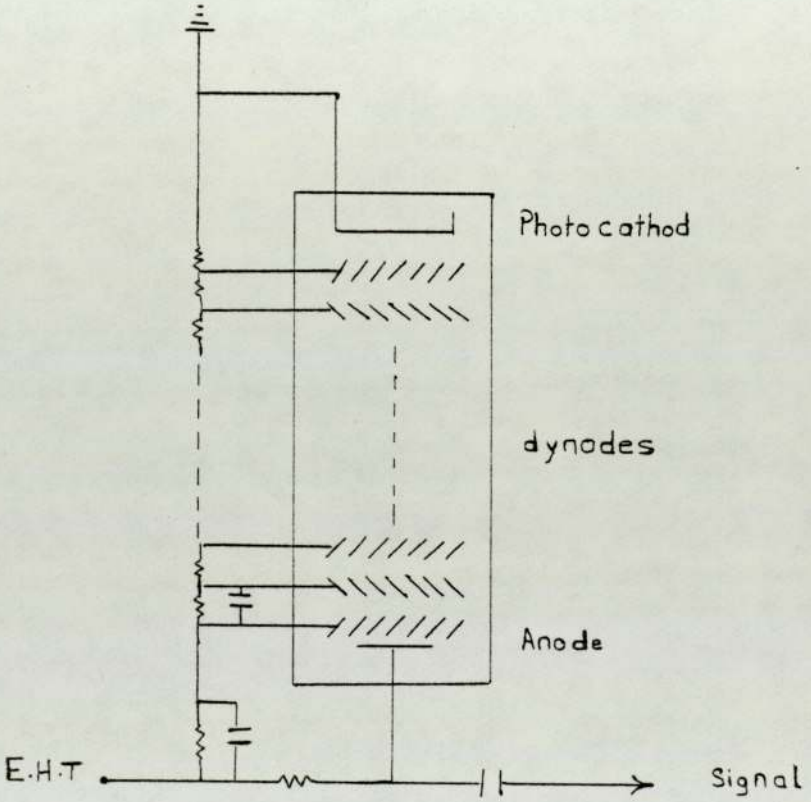

Fig 2.1o Circuit diagram showing potentiometer chain for supplying dynode potentials

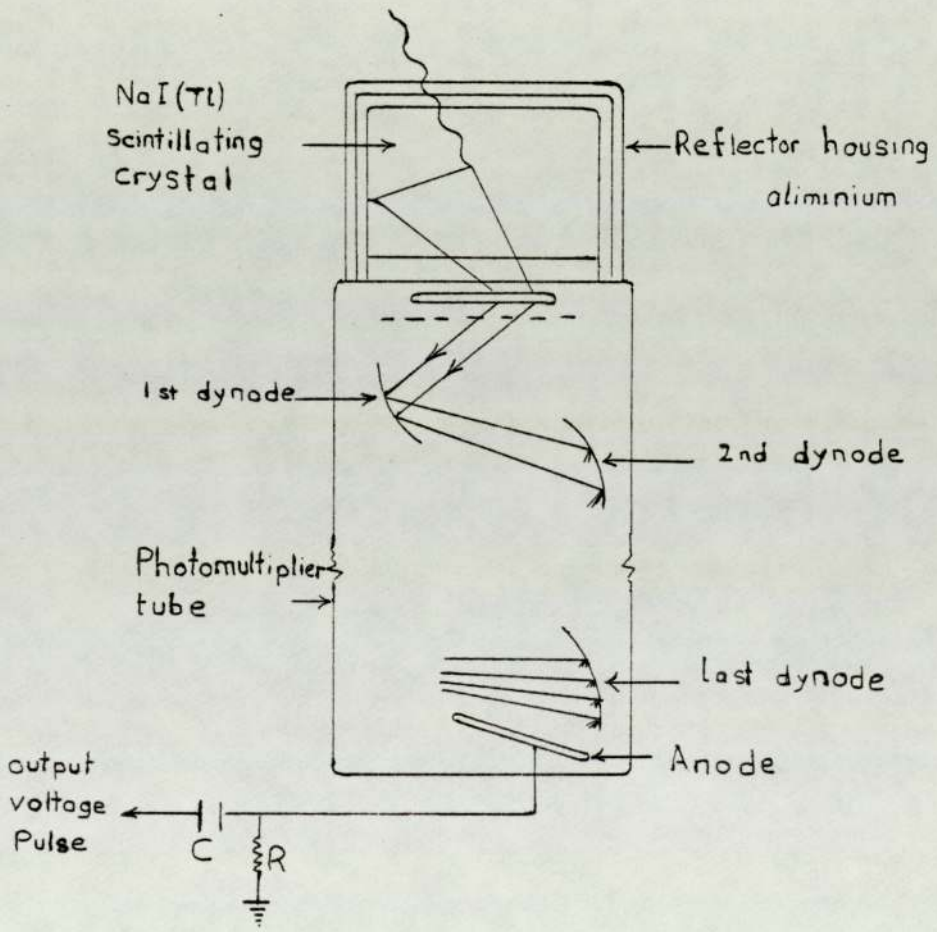

Fig 2.11 A NaI(Tl) Scintilation Crystal optically coupled to a photomultiplier tube

electrons appears at the anode. The photocathode and dynode voltages in the photomultiplier were obtained from a high voltage supply.

The block diagram below illustrates an electronic arrangement employed in this work.

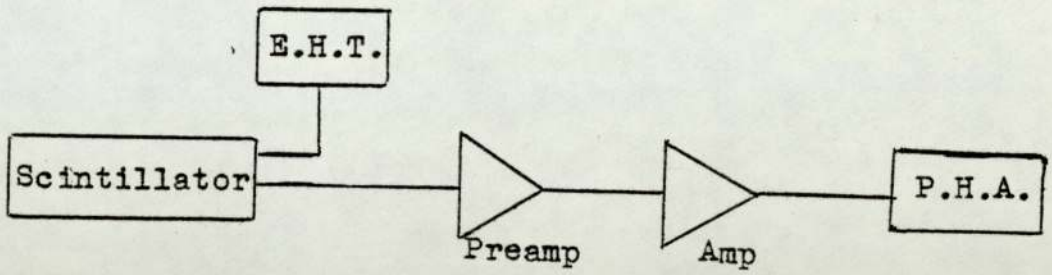

NaI(Tl) in general has several attractive properties. The crystal has a high density (3·67 g/cm^3) giving efficient absorption of the γ-radation. The decay constant is about 0·25 microseconds, which allows counting of a very high activity sample with small dead-time loss. NaI(Tl) can be grown into large single crystals and is very transparent to its fluorescent light, but it is hygroscopic, and therefore the crystal must be hermetically sealed in a closed container with an optical coupler to the photo-multiplier tube.

The resolution of the detection system is a measure of the ability of the detector system to produce a single pulse height value from monoenergetic radiation totally absorbed in the detector. The resolution per cent, R, is defined as the width of the total energy peak in the pulse height spectrum at half of the peak maximum.

$$R = \frac{\Delta E}{E} \times 100\ \% \qquad \text{(II.4.10)}$$

where E is the total γ-ray energy

ΔE is the energy interval for the full width at half

the maximum value of the peak (FWHM), Fig. 2.12. The resolution changes with γ -ray energy, thus the resolution value of a detector must be given for a particular γ -ray energy.

Two types of NaI(Tl) crystal were used in this work, a cylindrical crystal N656, fig. 2.13, 3 ins diameter and 3 ins depth, and a well crystal type, N597, fig. 2.14, 1·75 ins diameter and 2 ins high. The counting assembly is shielded in all directions by 2.5 cm of lead.

A well-type detector is sometimes more convenient in activation analysis, especially when low activites are measured, the well detector has higher efficiency and lower background than the cylindrical one.

II.4.3 Semiconductor detectors

From the band theory of solids it can be shown that the atomic energy levels of the outer electrons in a solid, by the operation of exchange effects between the individual atoms, split into a large number of levels forming a band which occupies a certain width E in the energy level diagram, fig. 2.15. An electron in a given state is shared by all atoms and the solid is an insulator or conductor, depending on whether or not the last band occupied by electrons is filled. If it is filled, the number of electrons moving in two opposite directions is the same, so that the net current is zero. If it is not filled, in the absence of an electric field, the configuration of lowest energy also has an equal number of electrons moving in two opposite directions, so that again there is no net current. By the application of an electric field, however, one can make this distribution

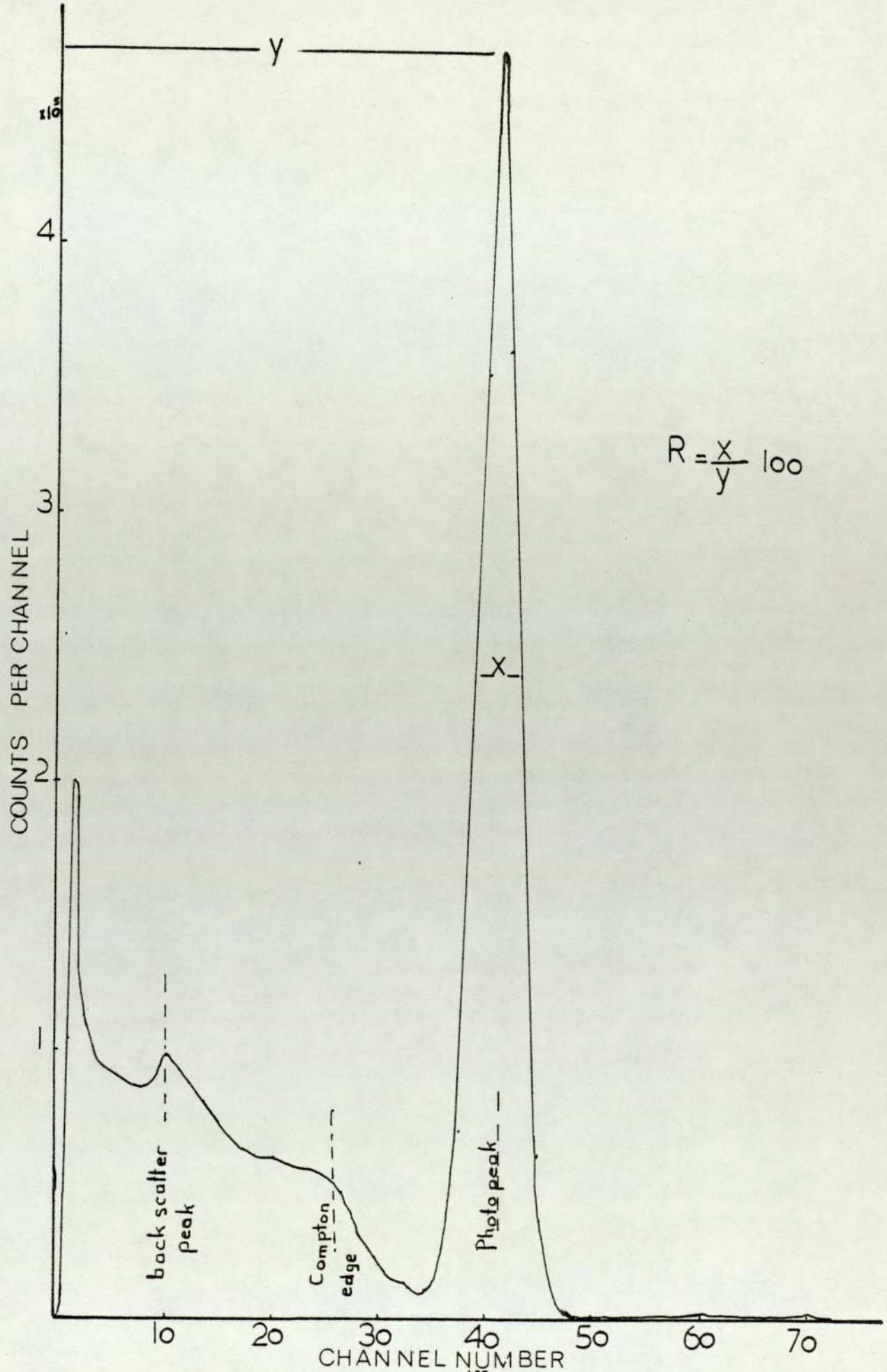

Fig (2.12) spectrum of ^{137}Cs

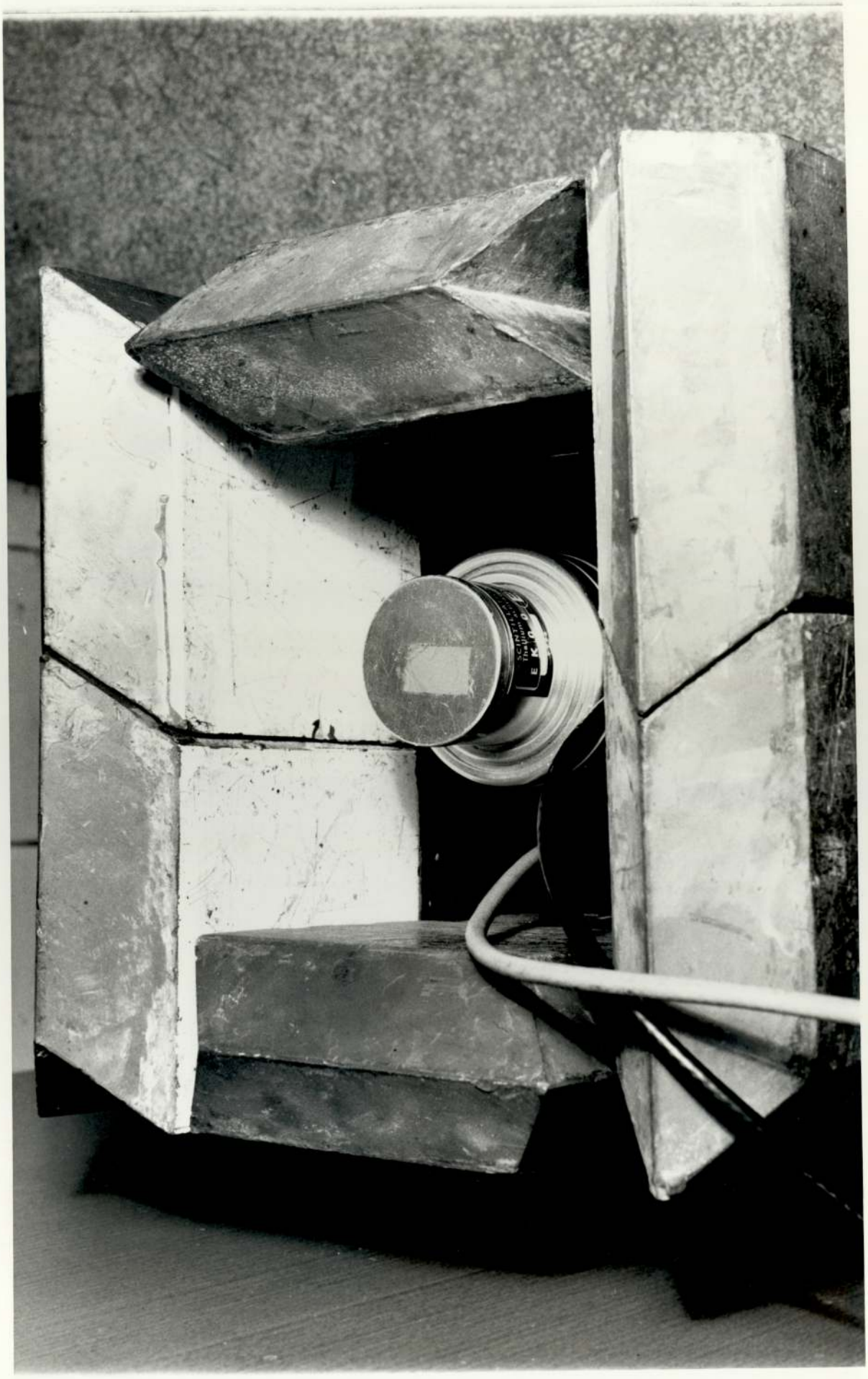

Fig 2.13

Fig 2.14

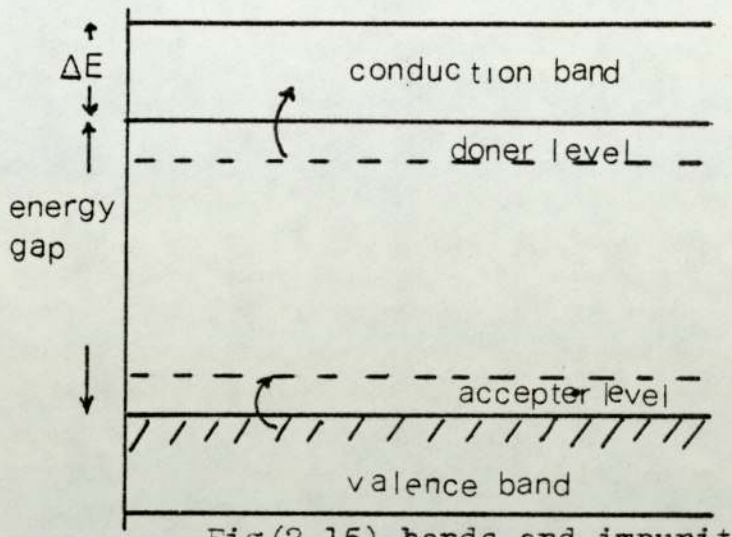

Fig(2.15) bands and impurity levels in semi-conductor

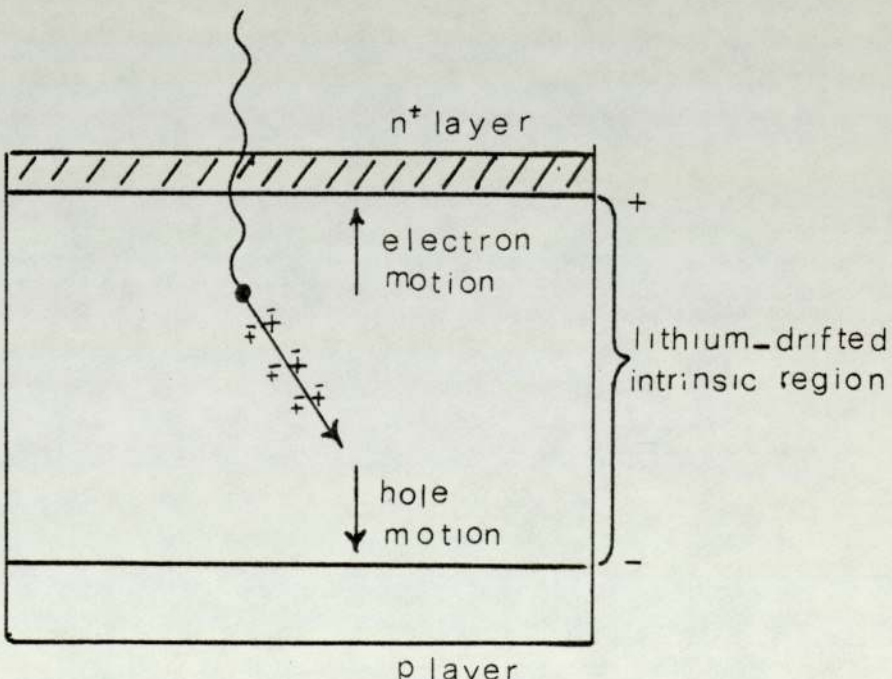

Fig (2.16) illustration of P-I-N planer structure of lithium ion drifted germanium detector

lopsided and produce a net current. This, then, is the situation in a conductor.

In an intrinsic semiconductor the gap between the last filled band, the valance band, and the next band, the so-called conduction band, is sufficiently small that by thermal excitation some electrons are lifted to the conduction band and thereby give the material a certain conductivity.

Another type of semiconductor has a relatively large gap between the two bands, but it contains impurities with energy levels close to the conduction band so that it is easier by thermal excitation to promote electrons up to the conduction band. In this N-type semiconductor, the current is transported by negative carriers produced by the donor impurity. Another possibility is that an acceptor impurity, that is, atoms with strong affinity for electrons because of vacancies, removes electrons from a lower filled band. The holes produced in the lower band represent positive charge carriers and the material is called a p-type semiconductor.

Referring again to fig. 2.15, one sees that the energy level due to the missing electrons in the p-type material lie close to, and can accept electrons from, the valence band.

In 1960 Pell demonstrated that lithium ions could be used to compensate for the presence of acceptor impurities in semiconductor materials. Using this technique, lithium ions are used to create a P-I-N structure such as shown in fig. 2.16.

These devices are fabricated by diffusing lithium

into the surface of an ingot of p-type Si or Ge, that is, Si or Ge with an acceptor type impurity which produces positive charge carriers, forming an n-type (donor type) region on one surface. A bias voltage is then applied to the ingot at high temperature causing the lithium ions to drift through the p-type material. During this process, an equilibrium condition is established where lithium ions pair with atoms of doping material (Ge or In in case of p-type Ge) creating a region with intrinsic properties. Under reverse bias, the charge carriers can then be collected from this region, resulting in the production of a solid state ionization chamber with appreciable volume.

Ge(Li) detectors are cooled to liquid nitrogen temperature because at room temperature lithium ions diffusion is still appreciable in Ge.

When a gamma ray strikes the intrinsic region and interacts, the ionization produced by the secondary electron generates electron-hole pairs which are rapidly collected at the electrodes, giving rise to a voltage pulse proportional to the number of pairs formed and therefore to the energy of the ectrons, assuming that the electrons released in photoelectric, Compton or pair production process are completely stopped in the intrinsic region. The greater the volume of the intrinsic region, the greater the detection efficiency.

An important advantage of the P-I-N detector over the scintillation detector is that the energy necessary to create an electron-hole pair is only about 3 eV, while an energy expenditure of at least 300 eV in a NaI(Tl)

crystal is needed to release one photoelectron from one cathode of the associated photomultiplier. Statistical fluctuations in the pulse production process are therefore proportionally much smaller for a solid state detector and the resolution of semiconductors is higher, the theoretical resolution, R, of a detector is given by[24]

$$R = 2{\cdot}355 \sqrt{F\, E\, \epsilon} \qquad \text{(II.4.11)}$$

where E is the energy of the γ -ray in KeV

ϵ is the average energy in eV to produce an electron -hole pair

F is the Fano factor which is related to the fractional amount of total energy absorbed in the production of electron-hole pairs.

The much better resolution of the solid state detector may be offset by its lower efficiency. The higher atomic number of iodine gives the NaI(Tl) scintillation detector a considerably greater photoelectric efficiency at higher energies. The difference in efficiency as a function of energy for Ge(Li) and NaI(Tl) detectors is shown in fig. 2.17.

The larger active volume of these counters also means that multiple Compton events can contribute appreciably to the counts within the full energy peak. Fig. 2.18 illustrates the difference between NaI and Ge(Li) detectors.

After the detailed explanation of NaI(Tl) scintillation and the semiconductor detectors, one can summarise the difference between them. According to the γ energy one is working with for better efficiency one has to use the NaI(Tl) detectors, but for the much better resolution the

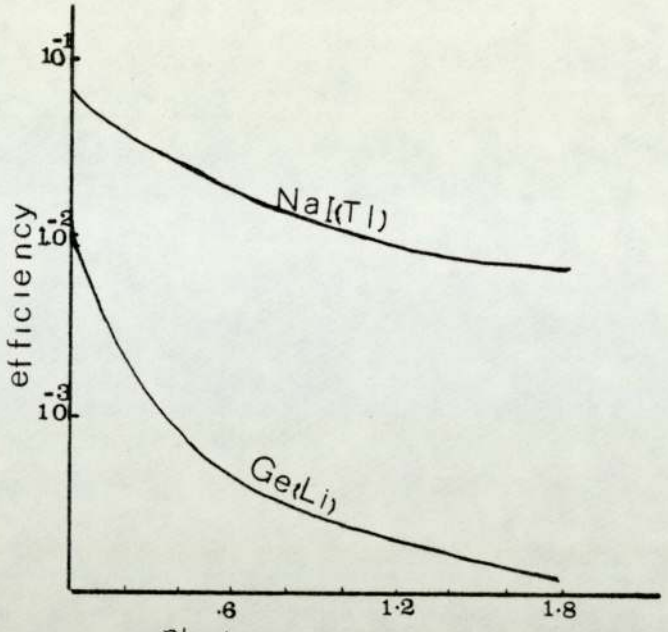

Fig(2.17) photopeak efficiency curves
20 cm^3 Ge(Li) detector
10 cm NaI(Tl) well crystal

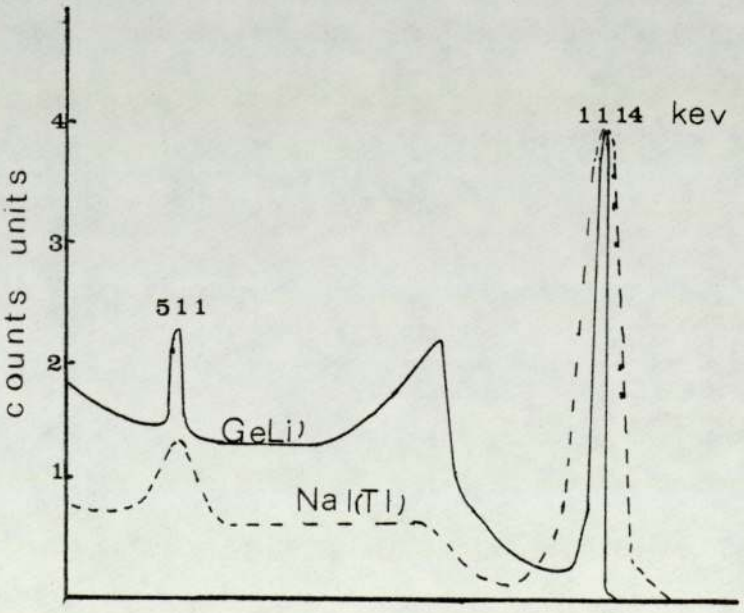

Fig(2.18) γ- spectra of a ^{65}Zn source
47 cm^3 Ge(Li) detector
3"x3" NaI(Tl) crystal

semiconductor detectors.

II.4.4 Multichannel analyzer

The electronic component, the multichannel analyzer, MCA, is used to examine pulses from the detector and sort these voltage pulses into groups corresponding to the original γ-ray distribution reaching the detector. The proportional voltage output from the detector was connected to the input of the multichannel analyzer. The voltage pulses are feeble and must be amplified before they will cause the other circuits to function properly. These were therefore amplified by an external amplifier or the linear amplifier in the MCA. If an external amplifier is used the output of the amplifier must be adjusted to the input level required by the MCA.

Two types of MCA were used in this work, a gamma scope model 102 with 100 channels and an Ireland 500 MCA. The pulses were sorted in the analyzer into the 100 or 512 channels in different basic modes, two of them were used in this work, the pulse height analyzer, PHA, and multi-scaler, MS, modes. In the PHA mode the gammascope was used to analyze signals whose pulse height is proportional to electron energy, each pulse accepted by the MCA in the PHA mode is sorted into one of the channels depending upon its peak amplitude. In the MS mode the pulses were counted sequentially, into the 512 channels. The scaler mode was used primarily to indicate the decay times of short lived isotopes, where MCA was set to certain dwell time per channel depending on the half-life of the isotope under investigation. In the MS mode a single channel was used which was characteristic by:

a) The base line: the voltage which sets the minimum pulse height from the detector accepted for counting.

b) The window: the increment in voltage from the base line voltage which sets the maximum pulse height accepted.

During accumulation the data may be presented on the gammascope, CRT, or on an external display oscilloscope, each count sorted in the memory channel was indicated on the display by a dot appearing in the channel. The level of the dot indicates the number of counts sorted in this particular channel. After accumulation was completed the data was read out to a typewriter, fig. 2.19.

Fig 2.19

CHAPTER III

ANALYSIS OF MEASUREMENTS

III.1 Derivation of expression for count rates

Fast neutrons obtained from the $^{3}T(d,n)^{4}He$ reaction on thick titanium-tritium targets were used to excite the sample, X, to form a nucleus which has an isomeric state, Y, with half-life $T_{½m}$ and decay constant λ_m, which decays to the ground state, Z, with half life $T_{½g}$ and decay constant λ_g.

This can be expressed as

$$X \longrightarrow Y \xrightarrow[\lambda_m]{\gamma} Z \xrightarrow[\lambda_g]{\beta,\gamma} C \qquad \text{(III.1.1)}$$

During the irradiation there was probability of interaction of X with the neutrons to form Y which subsequently decays to Z, i.e.

$$X \xrightarrow{\sigma_m} Y \xrightarrow{\lambda_m} Z \xrightarrow{\lambda_g} C \qquad \text{(III.1.2)}$$

At the same time there was a probability of interaction of X with the neutron to form Z directly, i.e.

$$X \xrightarrow{\sigma_g} Z \xrightarrow{\lambda_g} C \qquad \text{(III.1.3)}$$

where σ_m and σ_g are the cross-sections for the formulation of the isomeric and ground state respectively.

Let N be the number of atoms in the target sample, the rate of formation of Y depends on N, σ_m and ϕ, where ϕ is the neutron flux. During the time of irradiation, T, the net rate of formation of Y is given by[27]

$$\frac{dY_o}{dT} = \sigma_m N\phi - \lambda_m Y_o \qquad \text{(III.1.4)}$$

Integrating equation (III.1.4) gives, assuming that the flux is constant

$$Y_o = \frac{\sigma_m N\phi}{\lambda_m}\left[1 - e^{-\lambda_m T}\right] \qquad \text{(III.1.5)}$$

The rate of formation of Z, directly by the fast neutrons, and indirectly by disintegration of Y, is given by

$$\frac{dZ_o}{dT} = \sigma_g N\phi - \lambda_g Z_o + \lambda_m Y_o \qquad \text{(III.1.6)}$$

using equation (III.1.5)

$$\frac{dZ_o}{dT} = \sigma_g N\phi - \lambda_g Z_o + \sigma_m N\phi(1 - e^{-\lambda_m T}) \qquad \text{(III.1.7)}$$

equations (III.1.7) can be written in the form

$$\frac{dZ_o}{dT} + \lambda_g Z_o = \sigma_g N\phi + \sigma_m N\phi(1 - e^{-\lambda_m T}) \qquad \text{(III.1.8)}$$

multiplying both sides of equation (III.1.8) by $e^{\lambda_g T}$,

$$\frac{d}{dT}(Z_o e^{\lambda_g T}) = \sigma_g N\phi\, e^{\lambda_g T} + \sigma_m N\phi\, e^{\lambda_g T} - \sigma_m N\phi e^{(\lambda_g - \lambda_m)T} \qquad \text{(III.1.9)}$$

Integrating w.r.t. T.

$$Z_o e^{\lambda_g T} = \sigma_g \frac{N\phi}{\lambda_g} e^{\lambda_g T} + \frac{\sigma_m N\phi}{\lambda_g} e^{\lambda_g T} - \frac{\sigma_m N\phi}{\lambda_g - \lambda_m} e^{(\lambda_g - \lambda_m)T} + C \qquad \text{(III.1.10)}$$

Using the initial conditions that $Z_o = o$ at $T = o$ to evaluate C we have

$$Z_o = \frac{\sigma_g N\phi}{\lambda_g} + \frac{\sigma_m N\phi}{\lambda_g} - \frac{\sigma_m N\phi}{\lambda_g - \lambda_m} e^{-\lambda_m T} - \frac{\sigma_g N\phi}{\lambda_g} e^{-\lambda_g T} - \frac{\sigma_m N\phi}{\lambda_g} e^{-\lambda_g T} + \frac{\sigma_m N\phi}{\lambda_g - \lambda_m} e^{-\lambda_g T} \qquad \text{(III.1.11)}$$

This can be written in the form

$$Z_o = \frac{\sigma_g N\phi}{\lambda_g}(1 - e^{-\lambda_g T}) + \frac{\sigma_m N\phi}{\lambda_g}(1 - e^{-\lambda_g T}) + \frac{\sigma_m N\phi}{\lambda_g - \lambda_m}(e^{-\lambda_g T} - e^{-\lambda_m T}) \qquad \text{(III.1.12)}$$

The total disintegration rate of Z, at any time, t, after the end of the irradiation is

$$R = \lambda_g Z_o e^{-\lambda_g t} + \frac{\lambda_m \lambda_g}{\lambda_g - \lambda_m} Y_o(e^{-\lambda_m t} - e^{-\lambda_g t}) \qquad \text{(III.1.13)}$$

Substituting for Z_o and Y_o from (III.1.12) and (III.1.5) in equation (III.1.13), we get

$$R = \sigma_g N\phi\, e^{-\lambda_g t}(1 - e^{-\lambda_g t}) + \sigma_m N\phi\, e^{-\lambda_g t}(1 - e^{-\lambda_g T}) + \frac{\sigma_m N\phi \lambda_g}{\lambda_g - \lambda_m} e^{-\lambda_g t}(e^{-\lambda_g T} - e^{-\lambda_m T}) + \frac{\sigma_m N\phi}{\lambda_g - \lambda_m} \lambda_g e^{-\lambda_m t}(1 - e^{-\lambda_m T}) - \frac{\sigma_m N\phi}{\lambda_g - \lambda_m} \lambda_g e^{-\lambda_g t}(1 e^{-\lambda_m T}) \quad \text{(III.1.14)}$$

which can be written in the form

$$R = \sigma_g N\phi\, e^{-\lambda_g t}(1 - e^{-\lambda_g T}) + \sigma_m N\phi \left[\frac{\lambda_g}{\lambda_g - \lambda_m} e^{-\lambda_m t}(1 - e^{-\lambda_m T}) - \frac{\lambda_m}{\lambda_g - \lambda_m} e^{-\lambda_g t}(1 - e^{-\lambda_g T}) \right] \quad \text{(III.1.15)}$$

Equation (III.1.15) can be written in the form

$$R_s = X'.(A_s - B_s) + Y'.D_s \quad \text{(III.1.16)}$$

where

$$X' = \sigma_m N\phi$$

$$Y' = \sigma_g N\phi$$

$$A_s = \frac{\lambda_g}{\lambda_g - \lambda_m} e^{-\lambda_m t}(1 - e^{-\lambda_m T})$$

$$B_s = \frac{\lambda_m}{\lambda_g - \lambda_m} e^{-\lambda_g t}(1 - e^{-\lambda_g T})$$

$$D_s = e^{-\lambda_g t}(1 - e^{-\lambda_g T})$$

Thus by observing the activity of an irradiated sample as a function of time and applying the method of least squares to fit an equation of the form (III.1.15), the values of X' and Y' can be found. The ratio of X' to Y' if ϕ constant gives the isomeric cross-section ratio.

III.2 Method of least squares

III.2.1 The principle of least squares may be expressed as follows:

The most probable value of any observed quantity is such that the sum of the squares of the deviations of the observations from this value is least.

III.2.2 Application of method of least squares

Curve fitting to a set of experimental data.

Suppose R_1, R_2, ... are the values of a measured quantity R corresponding to the values C_1, C_2, ... C_n and D_1, D_2, ... D_n of another quantities C and D, these variables being connected linearly by the equation

$$R_s = C_s.X' + D_s.Y' \qquad \text{(III.2.1)}$$

where s takes the values from 1 to n.

The method of least squares can be applied to find the values of X' and Y' that satisfy all the equations (III.2.1.) as closely as possible.

i.e. $$X'.C_s + Y'.D_s - R_s = \epsilon_s \qquad \text{(III.2.2)}$$

We can choose X' and Y' such that the sum of the squares of the errors (ϵ_s) least, thus

$$\sum_{s=1}^{n} \left[X'.C_s + Y'.D_s - R_s\right]^2 \text{ must be minimum} \qquad \text{(III.2.3)}$$

Differentiating (III.2.3) partially w.r.t. X' and w.r.t. Y' we get as necessary conditions for a minimum

$$\sum C_s.(X'.C_s + Y'.D_s - R_s) = 0 \qquad \text{(III.2.4)}$$

and

$$\sum D_s.(X'.C_s + Y'.D_s - R_s) = 0 \qquad \text{(III.2.5)}$$

(III.2.4) and (III.2.5) can be written in the form

$$[CC]\,X' + [CD]\,Y' - [CR] = 0 \qquad \text{(III.2.6)}$$

$$[DC]\,X' + [DD]\,Y' - [DR] = 0 \qquad \text{(III.2.7)}$$

where

$$[CD] = \sum_{s=1}^{n} C_s D_s \qquad \text{(III.2.8)}$$

X' and Y' can be found from equation (III.2.6) and (III.2.7) where

$$X' = \begin{vmatrix} [CR][DC] \\ [DR][DD] \end{vmatrix} \Big/ \begin{vmatrix} [CC][CD] \\ [CD][DD] \end{vmatrix} \qquad \text{(III.2.9)}$$

and

$$Y' = \begin{vmatrix} [CC][CR] \\ [DC][DR] \end{vmatrix} \Big/ \begin{vmatrix} [CC][CD] \\ [CD][DD] \end{vmatrix} \qquad \text{(III.2.10)}$$

III.3 Calculation of errors

On the applications of method of least squares. let us suppose that C_s and D_s are known accurately but the R_s are subject to experimental errors. The most probable values of X' and Y' were the solutions of the normal equations (III.2.6) and (III.2.7). Denoting these values by X'_o, Y'_o and writing

$$X'_o.C_s + Y'_o.D_s - R_s = F_s \qquad \text{(III.3.1)}$$

i.e. F_1, F_2, ... F_n are the residuals when the most probable values X'_o, Y'_o are substituted in the given equations (III.3.1), it has been shown that the standard error, α, to be expected in any expression

$$X'_o.C_s + Y'_o.D_s - R$$

is given by(28)

$$\alpha^2 = [FF]/(n - 2) \qquad \text{(III.3.2)}$$

Let $\alpha_{X'}$ and $\alpha_{Y'}$ denote the standard errors in X'_o and Y'_o respectively, then it can be shown that

$$\frac{\alpha^2_{X'}}{[DD]} = \frac{\alpha^2_{Y'}}{[CC]} = \frac{\alpha^2}{\Delta} \qquad \text{(III.3.3)}$$

where

$$\Delta = \begin{vmatrix} [CC] & [CD] \\ [CD] & [DD] \end{vmatrix} \qquad \text{(III.3.4)}$$

Computer programmes were written toevaluate the isomeric ratio and standard errors. Appendix (1) and (2).

III.4 Calculations for optimum time of irradiation

It was assumed that the optimum time of irradiation required for good results of the isomeric ratio was the time at which the activity of the isomeric state is equal to the activity of the ground state, i.e.

$$\lambda_m Y_o = \lambda_g Z_o \qquad \text{(III.4.1)}$$

Y_o and Z_o are given by equations (III.1.5) and (III.1.12) therefore

$$\bar{\sigma}_m N\emptyset(1 - e^{-\lambda_m T}) = \bar{\sigma}_g N\emptyset(1 - e^{-\lambda_g T}) + \bar{\sigma}_m N\emptyset(1 - e^{-\lambda_g T}) + \bar{\sigma}_m N\emptyset \frac{\lambda_g}{\lambda_g - \lambda_m}(e^{-\lambda_g T} - e^{-\lambda_m T}) \qquad \text{(III.4.2)}$$

where

$N\emptyset$ is constant

Using $e^{-X} = 1 - X + \frac{X^2}{2!} \ldots$

Equation (III.4.2) can be written as

$$\bar{\sigma}_m\left[\lambda_m T - \lambda_m \frac{T^2}{2} + \ldots\right] = \bar{\sigma}_g\left[\lambda_g T - \lambda_g^2 \frac{T^2}{2} + \ldots\right] + \bar{\sigma}_m\left[\lambda_g T - \lambda_g^2 \frac{T^2}{2} + \ldots\right] + \frac{\bar{\sigma}_m \lambda_g}{\lambda_g - \lambda_m}\left[\lambda_m T - \lambda_g T + \frac{\lambda_g^2 T^2}{2} - \frac{\lambda_m^2 T^2}{2} + \ldots\right] \qquad \text{(III.4.3)}$$

Keeping the leading terms only, equation (III.4.3) will be

$$\bar{\sigma}_m \lambda_m T - \bar{\sigma}_m \lambda_m^2 T^2 = \bar{\sigma}_g \lambda_g T - \bar{\sigma}_g \frac{\lambda_g^2 T^2}{2} + \bar{\sigma}_m \lambda_g T - \frac{\bar{\sigma}_m \lambda_g^2 T^2}{2} + \bar{\sigma}_m \lambda_g \frac{(\lambda_m - \lambda_g)T}{\lambda_g - \lambda_m} + \frac{\bar{\sigma}_m \lambda_g}{2(\lambda_g - \lambda_m)}(\lambda_g - \lambda_m)(\lambda_g + \lambda_m)T^2 \qquad \text{(II.4.4)}$$

Equation (III.4.4) can be written as

$$2(\bar{\sigma}_m \lambda_m - \bar{\sigma}_g \lambda_g) = \left[\bar{\sigma}_m \lambda_m^2 - \bar{\sigma}_g \lambda_g^2 + \bar{\sigma}_m \lambda_m \lambda_g\right] T \qquad \text{(III.4.5)}$$

Therefore the optimum time of irradiation T is given by

$$T = \frac{2\left[\frac{\sigma_m}{\sigma_g}\lambda_m - \lambda_g\right]}{\left[\frac{\sigma_m}{\sigma_g}\lambda_m^2 - \lambda_g^2 + \frac{\sigma_m}{\sigma_g}\lambda_m\lambda_g\right]} \qquad \text{(III.4.6)}$$

The optimum time of irradiation, T, was calculated using equation (III.4.6) for the reaction $^{45}Sc(n,2n)^{44m,g}Sc$, $^{76}Ge(n,2n)^{75m,g}Ge$, $^{113}In(n,2n)^{112m,g}In$, and $^{198}Pt(n,2n)^{197m,g}Pt$. The results are shown in Table II.

TABLE II

Sample	Isomeric ratio used in the calculation	T
$^{44m,g}Sc$	0.80	11.4 h
$^{75m,g}Ge$	4.00	2.3 m
$^{112m,g}In$	5.00	21.0 m
$^{197m,g}Pt$	0.68	8.9 h

It was not always possible to achieve optimum times for practical reasons.

III.5 The effect of the change of the flux during the irradiation on isomeric ratio

If the incident neutron flux, $\emptyset$, remains constant till the end of the time of irradiation, T, then the activity of the isomeric state, A_m, is given by

$$A_m = \sigma_m N\emptyset(1 - e^{-\lambda_m T}) \qquad \text{(III.5.1)}$$

and the activity of the ground state, A_g, is given by

$$A_g = \sigma_g N\emptyset(1 - e^{-\lambda_g T}) + \sigma_m N\emptyset(1 - e^{-\lambda_g T}) + \sigma_m N\emptyset \frac{\lambda_g}{\lambda_g - \lambda_m}(e^{-\lambda_g T} - e^{-\lambda_m T}) \qquad \text{(III.5.2)}$$

The isomeric cross-section ratio can be determined using the two equations (III.5.1) and (III.5.2).

To study the effect of an unnoticed change of the flux during irradiation on the measured isomeric ratio values, the apparent isomeric ratio will be calculated for two cases of the flux change, fig. 3.1 and fig. 3.2, and compare them with the case of the steady flux.

Case 1. If the flux, Ø, dropped by 10% during the first half time of irradiation as represented in diagram III.1

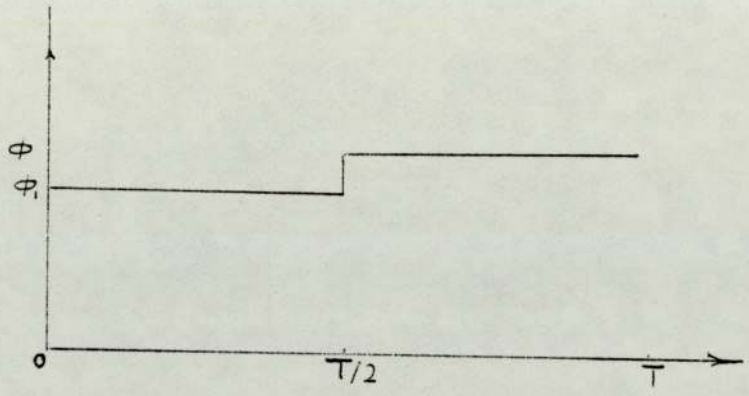

diagram III.1

where

$$\emptyset_1 = 0.9\ \emptyset$$

At the end of irradiation, T, the activity of the isomeric state is given by

$$A_{m_1} = \sigma_m N\emptyset\left(1 - e^{-\lambda_m \frac{T}{2}}\right)\left(1 + \cdot 9\ e^{-\lambda_m \frac{T}{2}}\right) \qquad (III.5.4)$$

the activity of the ground state is given by

$$A_{g_1} = (\sigma_m+\sigma_g)N\emptyset\left(1 - e^{-\lambda_g \frac{T}{2}}\right)\left(1 + \cdot 9\ e^{-\lambda_g \frac{T}{2}}\right)$$
$$+ \sigma_m N\emptyset \frac{\lambda_g}{\lambda_g-\lambda_m}\left(e^{-\lambda_g \frac{T}{2}} - e^{-\lambda_m \frac{T}{2}}\right)\left[0{\cdot}1 + 0{\cdot}9\left(e^{-\lambda_g \frac{T}{2}} + e^{-\lambda_m \frac{T}{2}}\right)\right] \qquad (III.5.5)$$

The results for the apparent isomeric cross-section ratio calculated using the two equations (III.5.4) and (III.5.5) deviate from that with constant flux Ø by about 1% for

$^{112m,g}In$ and $^{44m,g}Sc$. If the flux dropped to the extreme, at which $\phi_1 \simeq 0$, in the first half of irradiation the deviation will increase to 20% in the case of $^{112m,g}In$ and 10% for the $^{44m,g}Sc$.

Case II. If the flux, ϕ, decreased by 10% during the second half time of irradiation as in diagram III.2

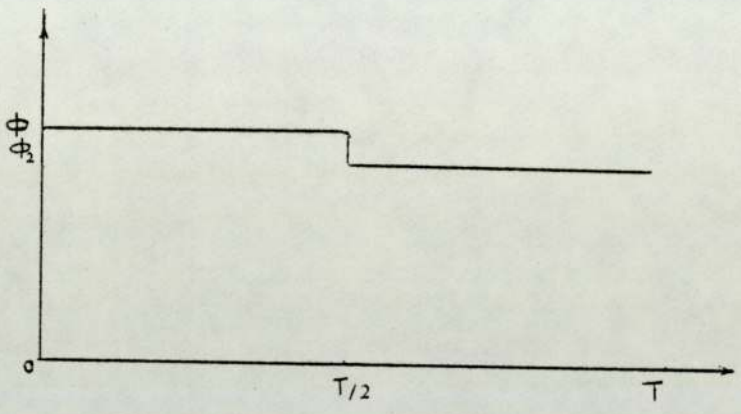

diagram III.2

where

$$\phi_2 = 0.9\ \phi$$

At the end of irradiation, T, the activity due to isomeric state is given by

$$A_{m_2} = \sigma_m N\phi(1 - e^{-\lambda_m \frac{T}{2}})\ (0.9 + e^{-\lambda_m \frac{T}{2}}) \qquad \text{(III.5.7)}$$

and the activity due to the ground state is

$$A_{g_2} = (\sigma_m + \sigma_g)\ N\phi(1 - e^{-\lambda_g \frac{T}{2}})\ (0.9 + e^{-\lambda_g \frac{T}{2}})$$
$$+ \sigma_m N\phi \frac{\lambda_g}{\lambda_g - \lambda_m} (e^{-\lambda_g \frac{T}{2}} - e^{-\lambda_m \frac{T}{2}})\ (e^{-\lambda_g \frac{T}{2}} + e^{-\lambda_m \frac{T}{2}} - 0.1) \qquad \text{(III.5.8)}$$

The isomeric cross-section ratio was calculated using equations (III.5.7) and (III.5.8), the deviation was about 2% for In and Sc from that calculated with steady flux. If the flux dropped in the second half of irradiation to the extreme, i.e. with $\phi_2 \simeq 0$, this deviation will increase to

25% in the case of $^{112m,g}In$ and 30% for $^{44m,g}Sc$. The two extreme cases did not happen in this measurement, the effect of a little change in the flux will not be more than 2%.

CHAPTER IV

RESULTS

4.1 Typical measurements

As explained before, the general approach in measuring the isomeric cross-section was as follows. Fast neutrons were obtained from the $^{3}T(d,n)^{4}He$ reaction in thick titanium-tritium targets. The sample was placed beside the target for irradiation, and subtended certain angles at the target with respect to the deuteron beam direction. The deuteron energy was about 300 KeV. The irradiated sample was then transferred to the selected detector whose signal feeds into the multichannel analyzer.

To determine the isomeric cross-section ratio, the analyzer was set to acquire counts arising from the ground state activity for fixed time intervals. At the end of each counting interval, the data was fed to a teletype printer, the analyzer was cleared and set to repeat the data accumulation. The acquire and print-out process continued until a sufficiently large number of measurements had been made.

The time behaviour of the activity was then matched to the equation III.1.16. By using the experimental yields for a large number of different time intervals and this equation the coefficients X' and Y' were determined by application of the method of least squares, using the computer programme, appendix 1. The ratio of X' to Y' then yields the isomeric cross-section ratio. The reactions $^{45}Sc(n,2n)^{44m.g}Sc$, $^{113}In(n,2n)^{112m.g}In$, $^{198}Pt(n,2n)^{197m.g}Pt$, and $^{76}Ge(n,2n)^{75m.g}Ge$ were studied.

4.2 Decay schemes

A decay scheme is a representation of the nuclear energy levels of a radionuclide and the modes of de-excitation. The decay scheme shows each mode of decay, its abundance, the energy of the radiations, the sequence of emissions, the half-lives involved, and the product nuclide. The lowest bar for each nuclide shows the nuclide in its lowest energy state, the ground state, even if the nuclide is radioactive. Decay schemes vary from simple, involving only one mode of decay, to complex, with two or more modes of decay or by one mode to many energy states. The latter are usually accompanied by several γ ray transitions. The decay scheme is important in radioactivity measurement since it relates the amount of radiation of a given kind and energy to the actual number of disintegrations of the particular radionuclide.

The decay schemes for $^{44m.g}Sc$, $^{75m.g}Ge$, $^{112m.g}In$, and $^{197m.g}Pt$ are illustrated in figures 4.1 and 4.2.

4.2.1 Decay scheme for $^{44m.g}Sc$ (25,26)

The (n,2n) reaction on ^{45}Sc leads to two isomeric states of ^{44}Sc, the 2·44 day metastable state of ^{44m}Sc is 0·271 MeV above the 3·92 hour ^{44g}Sc. ^{44m}Sc decays to ^{44g}Sc by an isomeric transition, IT, in 98·6% of disintegrations and electron capture, EC, to ^{44}Ca accounts for the remaining 1·4% of the disintegrations.

^{44g}Sc decays by both positron emission, 94% of the disintegrations, and EC, 5·9% of the disintegrations, of which 0·9% result in the 2·66 MeV and 5% result in the 1·156 MeV excited state of ^{44}Ca. Thus for each 100 disintegrations of ^{44g}Sc there would be available for

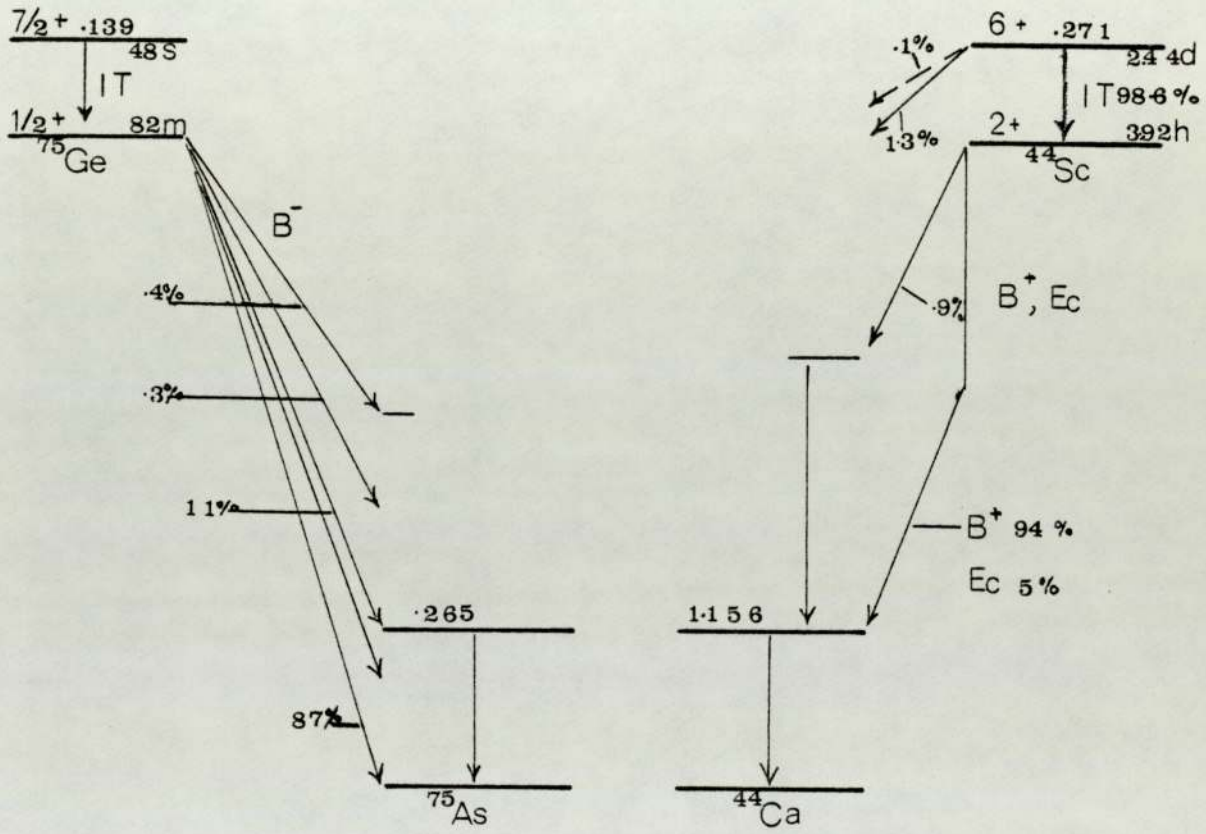

Decay Scheme For ^{75}Ge Decay Scheme For ^{44}Sc

Fig. 4·1

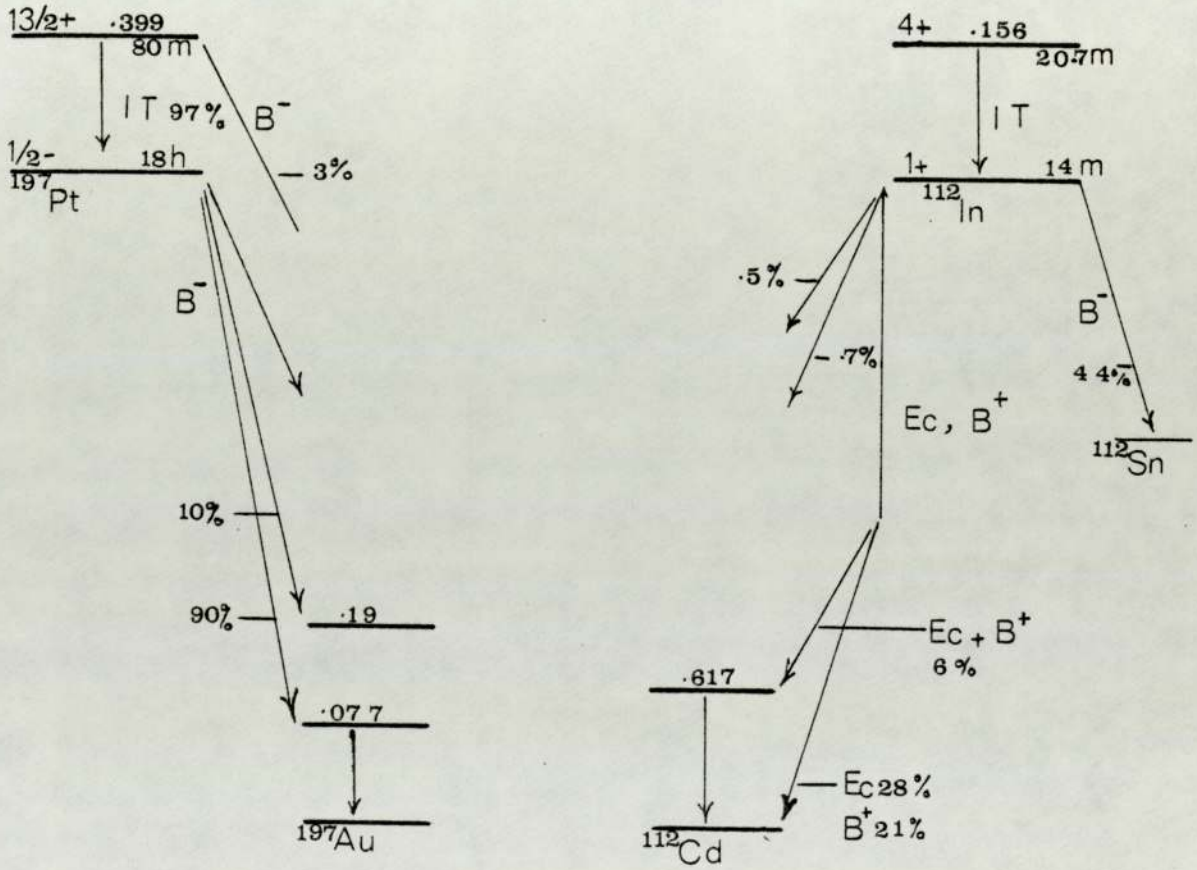

Decay Scheme For ^{197}Pt Decay Scheme For ^{112}In

Fig. 4.2

measurement 94 positrons, 188 annihilation photos of 0·511 MeV, 0·9 γ rays of 1·5 MeV, and 5 gamma rays of 1·156 MeV.

^{44g}Sc is most easily measured by observing the 0·511 MeV annihilation photons.

4.2.2 Decay scheme for $^{75m.g}$Ge (29,30)

The (n,2n) reaction of ^{76}Ge leads to two isomeric states of ^{75}Ge, the 48 s metastable state of ^{75m}Ge is 0·139 MeV above the 82 m ^{75g}Ge. For practical purposes the 48 s activity could be measured by the isomeric transition, IT, gamma rays of 0·139 MeV being released as ^{75m}Ge decays to ^{75g}Ge.

The decay scheme for 82 m ^{75g}Ge shows five beta decay branches, four resulting in excited states and the fifth in the ground state of the product nuclide, ^{75}As. Since each of the excited states decays to the one below it, each 100 disintegrations of ^{75g}Ge would yield, in addition to the beta particles 0·4 gamma ray with E_γ = 0·151 MeV, 0·7 γ ray with E_γ = 0·212 MeV, and 11·7 γ ray with E_γ = 0·265 MeV. ^{75g}Ge could be measured by observing the 0·265 MeV gamma ray.

4.2.3 $^{112m.g}$In decay scheme (31,32)

The (n,2n) reaction of ^{113}In leads to two isomeric states of ^{112}In, the 20·7 m metastable state of ^{112m}In is 0·156 MeV above the 14 m ^{112g}In. ^{112m}In decays to ^{112g}In by an IT γ ray of 0·156 MeV.

The decay scheme of ^{112g}In shows that it decays by three modes, electron capture and positron emission to ^{112}Cd with four branches totalling 56%, and beta emission,

one branch of 44%, to the ground state of ^{112}Sn. Each 100 disintegrations would yield 44 gamma rays of 0·511 MeV and 7·2 of 0·617 MeV. The isotope could be measured by observing the 0·511 photons or the three beta branches by a beta counter.

4.2.4 $^{197m.g}Pt$ decay scheme (33,34)

The (n,2n) reaction of ^{198}Pt leads to two isomeric states of ^{197}Pt, the 80 m metastable state ^{197m}Pt is 0·399 MeV above the 18 h ^{197g}Pt. ^{197m}Pt decays by IT, 97%, to ^{197g}Pt and β^- 3% to ^{197}Au. For practical purposes the 80 m activity could be measured by the isomeric transition gamma ray of 0·346 MeV released as ^{197m}Pt decays to ^{197g}Pt.

The decay scheme for 18 h ^{197g}Pt shows two beta decay branches resulting in excited states of the product nuclide, ^{197}Au. Each 100 disintegrations of ^{197}Pt would yield in addition to the 10 and 90 beta particles 10 γ rays with energies 0·19 MeV and 100 γ rays with energy 0·077 MeV. ^{197g}Pt could be measured by observing the 0·19 MeV because 77 KeV near X-rays.

4.3 Isomeric states investigated

4.3.1 The $^{45}Sc(n,2n)^{44m.g}Sc$ reaction

Samples of a few grams of scandium oxide (Analar, natural scandium is 100% ^{45}Sc) in powder form was irradiated for three hours. Each sample was in a plastic container of 8mm diameter and placed 3·9 cm from the tritium target. In this arrangement, for instance, the energy spread of the incident neutrons was ± 0·1 MeV if the sample was at 90° to the incident

beam. A typical spectrum immediately after irradiation is shown in fig. 4.3. The spectrum was studied and there was a little interference due to the reaction $^{45}Sc(n,\alpha)^{42}K$ which results in a peak in the ^{44}Sc spectrum at 1·5 MeV.

Samples were irradiated at angles 0°, 90° and 155° to the incident beam. The energies of the neutrons at these angles were 15·37 ± 0·01, 14·14 ± 0.1 and 13·12 ± 0·04 MeV. After irradiation the activity of 0·511 MeV annihilation photons line was followed, using the 3" x 3" NaI(Tl) detector, the interference due to ^{42}K was subtracted from the photopeak under investigation. For background subtraction a base line extrapolated between the channels adjacent to the peak is estimated, fig. 4.3.

The time behaviour of the decay of ^{44g}Sc which was produced directly by the (n,2n) reaction and from the decay of ^{44m}Sc was plotted on semi-logarithmic paper, a typical example is shown in fig. 4.4. Corresponding to large values of time near the end of the curve one found the experimental points to be on a straight line. A straight line passing through these points and extended to $t = 0$ was shown. Since the ground state has the shorter half-life, this straight line represented the decay of the isomeric state. The slope of the line gave the decay constant λ_m, from the decay constant the half-life of the isomeric state was determined, it was 58 h. From the experimental points the activity of the 58 h half-life represented by the straight line explained above was subtracted. The result of the subtraction is another straight line with slope equal to λ_g corresponding to

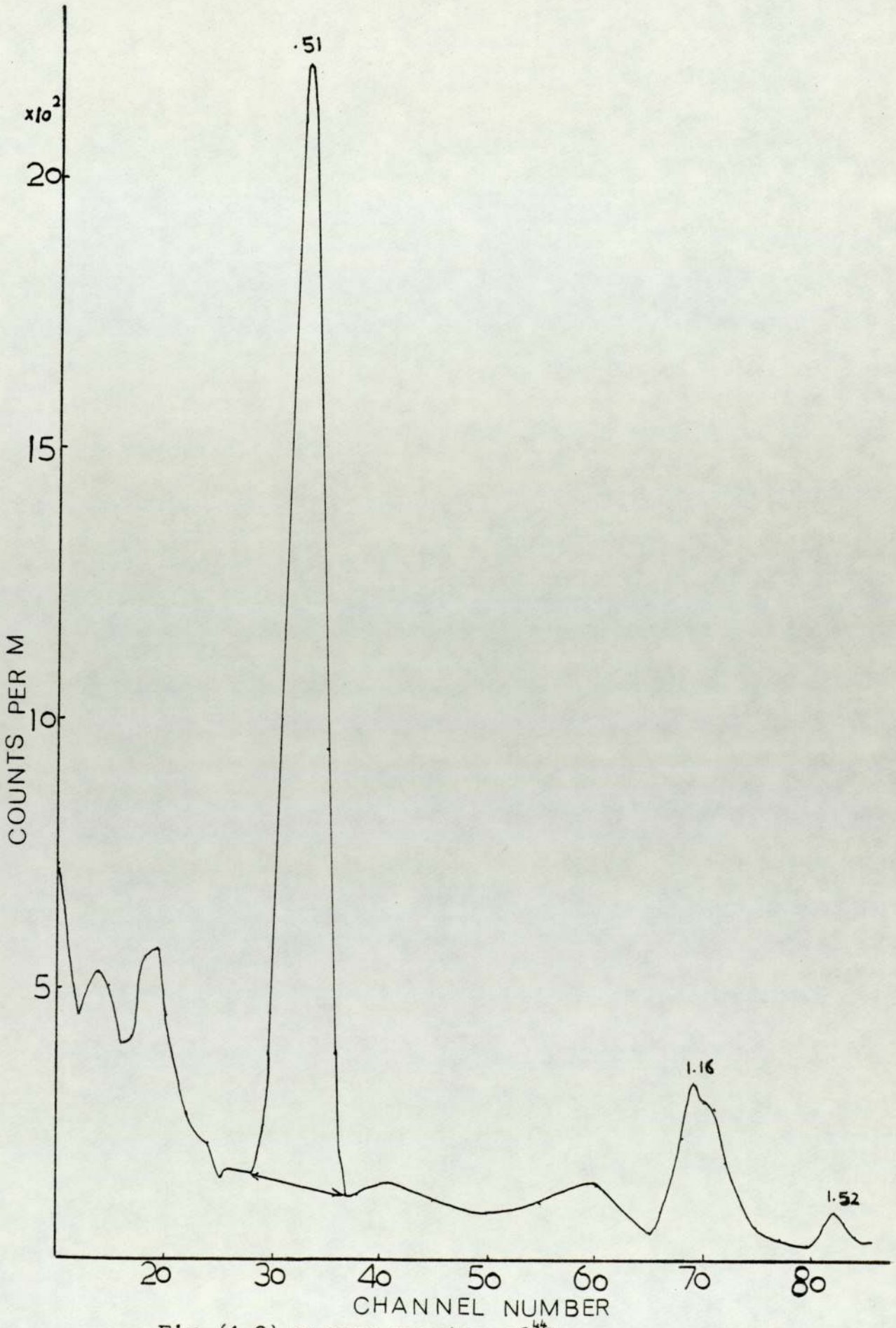

Fig (4.3) γ rays spectra of ^{44}Sc

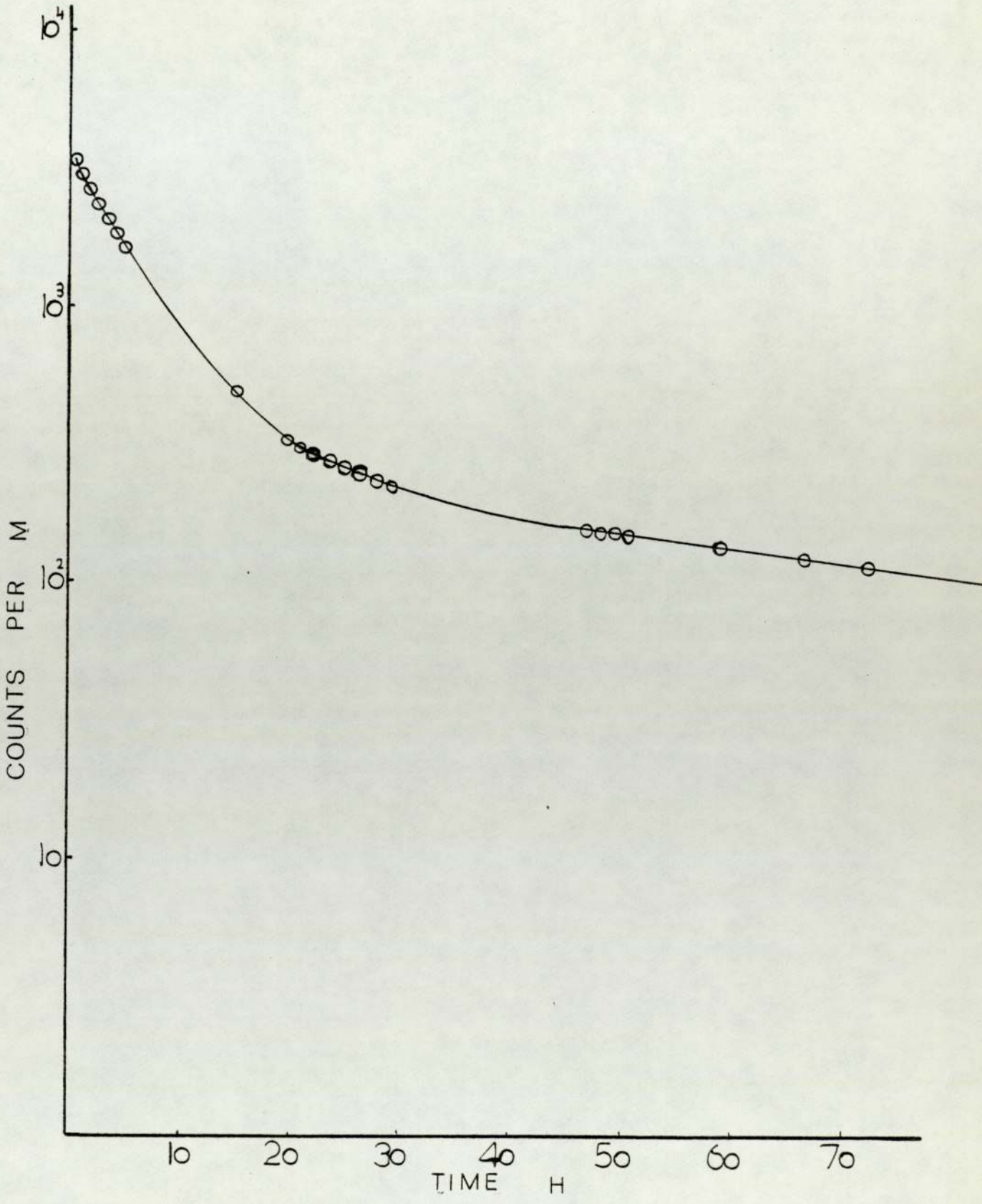

Fig(4.4) time behaviour of decay of ^{44}Sc

the ground state, the shorter half-life. $T_{½g}$ was found to be 3·92 h. These two half-lives are very close to the accepted figures, which indicates no unexpected interference was present in the activity of 511 KeV line.

For calculation of the isomeric cross-section ratio the time behaviour of the net activity was then matched to the equation III.1.16 the ratio of the coefficients X' to Y' was determined using the computer programme, appendix 1. The half-lives used were those taken from the table of isotopes.(35) The standard deviation on the isomeric ratio was calculated using a computer programme, appendix 2.

The results for ^{44}Sc are given in table II,1 each isomeric ratio value is the average of at least two runs at each neutron energy.

Results of the isomeric ratio as a function of neutron energy together with the values of other investigators are given in fig. 4.5.

The results of this work are in good agreement with the work of Rayburn(36), somewhat lower than the results of Eapen(15), higher than Kao(16) and the Karolyi(37) value, but far from Prasod(12) value, and the measurements of Prestwood.(38)

The present work should have good reliability because the results so obtained for the isomeric cross-section ratio are independent of several sensitive factors such as a photopeak detection efficiency, γ ray intensity, and absorption corrections. These factors invariably constitute the major portion of the uncertainty in the results of earlier experiments.

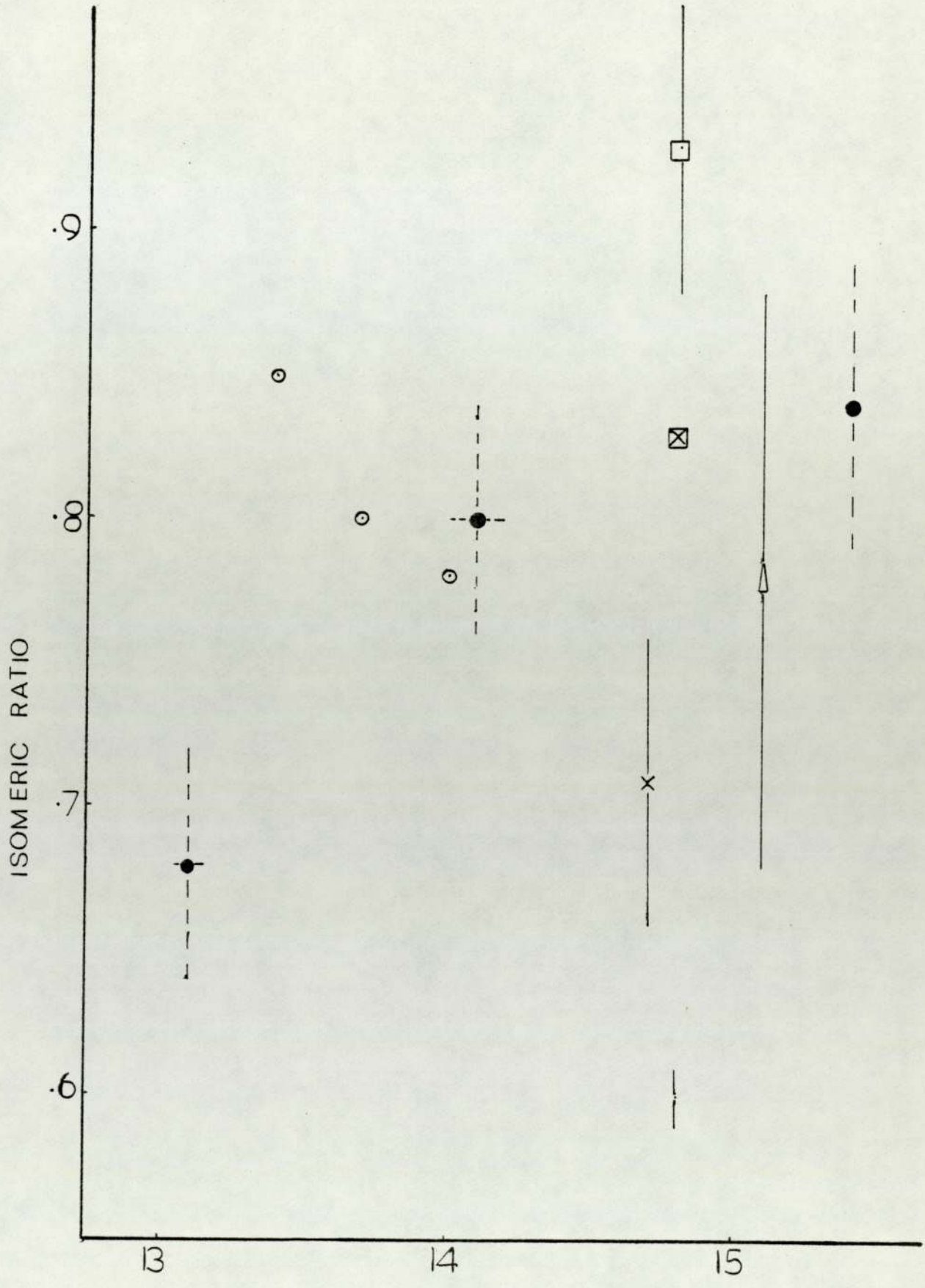

Fig(4.5) isomeric cross section ratio of $^{45}Sc(n,2n)^{44}Sc$ with values of other workers

• present work, ▫ ref(15), Δ ref(16), ⊠ ref(36), × ref(37), · ref(12), ○ ref(38)

Table II.1

Neutron energy MeV	Number of runs	Average value of isomeric ratio
13·12 ± 0·04	2	0·68 ± 0·04
14·14 ± 0·10	3	0·80 ± 0·04
15·37 ± 0·01	2	0·84 ± 0·07

Results for the reaction $^{45}Sc(n,2n)^{44m\cdot g}Sc$

4.3.2 $^{113}In(n,2n)^{112m,g}In$ reaction

A sample of a few grams of natural indium metal was irradiated for 15 minutes at a neutron energy of 14·14 MeV, natural indium consists of ^{113}In, 4·23% and ^{115}In, 95·77%. The sample was in a plastic container 8 mm in diameter and was placed 2·4 cm from the tritium target, in this arrangement the energy spread of the incident neutrons was ± 0·2 MeV.

The sample was surrounded with Cd sheet during irradiation to greatly reduce a large interference arising from $^{115}In(n,\gamma)^{116m}In$ reaction. Measurements have been made[39] of the flux of thermal neutrons near the target of the neutron generator. For a fast neutron output of 10^9 neutrons per second the measured thermal flux was $3·8 \times 10^4$ neutrons per cm^2 per second. Applying these values to the arrangement used together with the cross-sections and the abundances for the thermal and fast reactions one would expect about five times as much activity from thermal, this is greatly reduced by using cadmium. The rapid transfer system was used to transfer the sample to the detector.

As the ^{112}In activity was rather low, the well detector was tried first, the spectrum is shown in fig. 4.6. To obtain much better resolution the activity of the sample was measured using the Ge(Li) detector in a second run. The spectrum obtained is shown in fig. 4.7. The peak at 0·511 MeV due to the annihilation of β^+ particles resulting from the decay of the ground state of ^{112}In is clearly visible. There is no other reaction product other than this which will give β^+ particles.

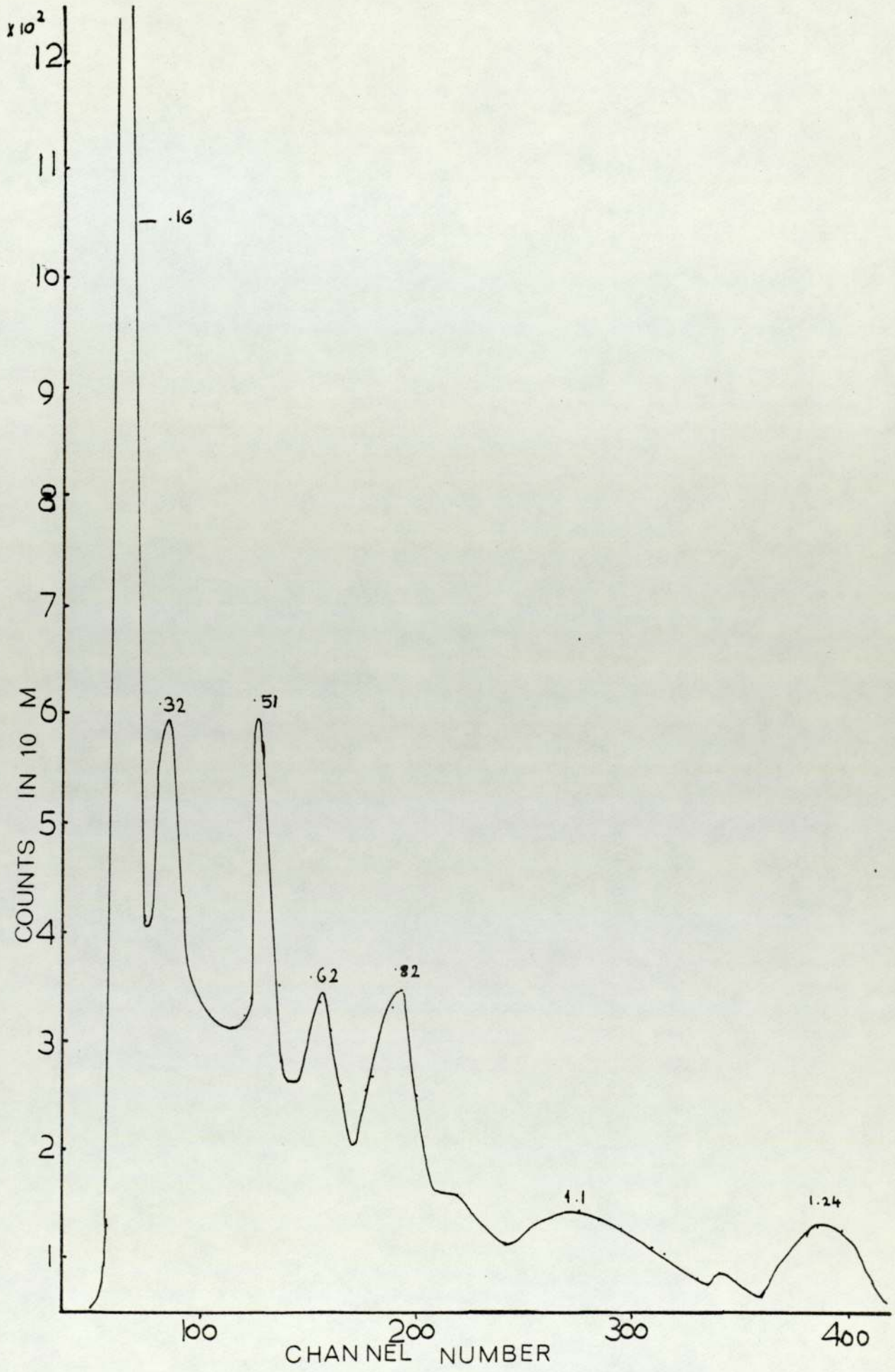

Fig (4.6) γ rays spectra of ^{112}In measured by NaI(Tl) detector

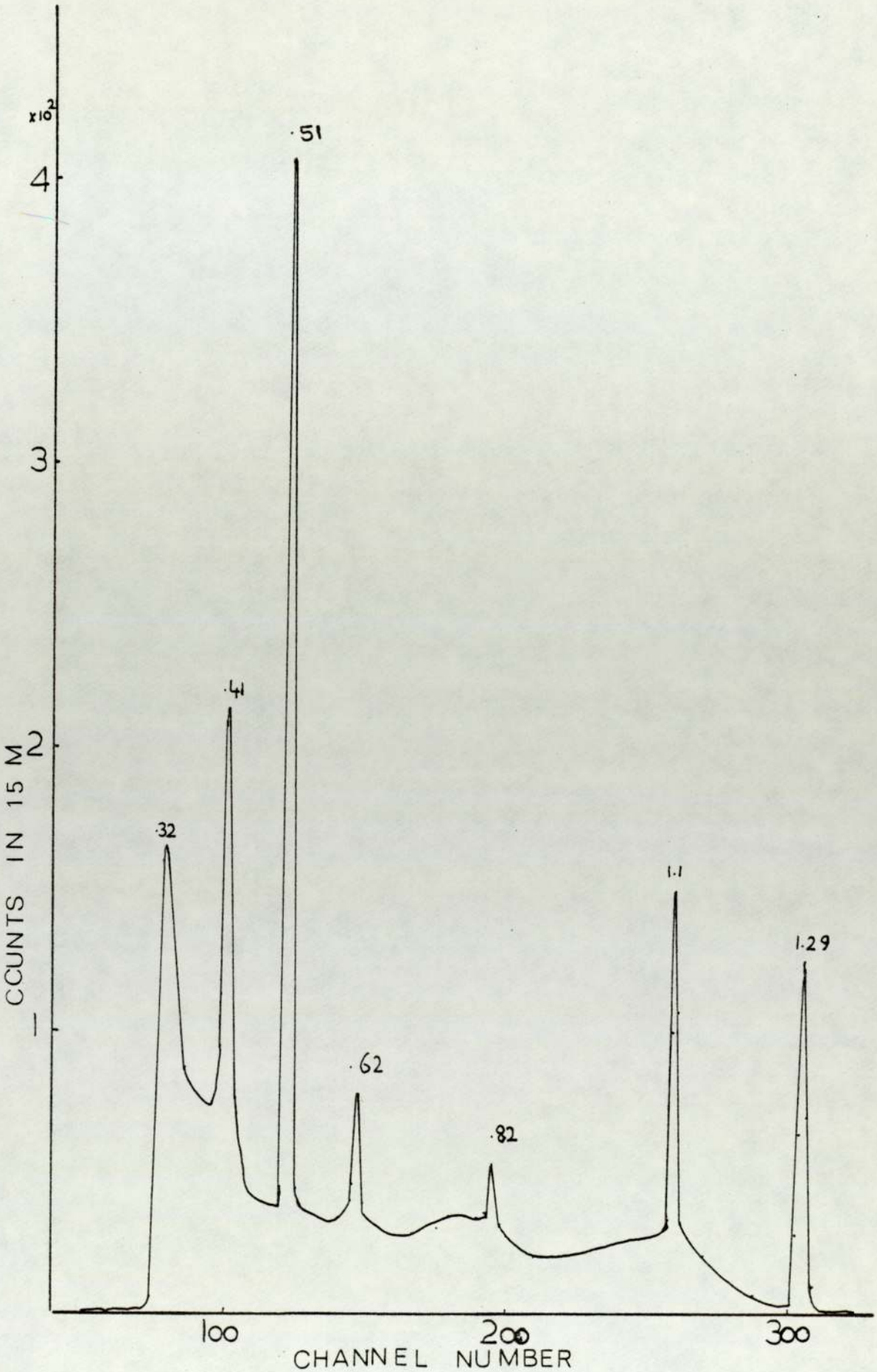

Fig (4.7) γ rays spectra of ^{112}In measured by Ge(Li) detector

However, there was some interference from ^{116m}In($T_{½}$=54 m) which results in the peaks at 0·82, 1·09 and 1·29 MeV and interference from ^{115m}In at 0·32 MeV.

For good accuracy it was better not to use the multiscale mode in following the decay of 0·511 MeV annihilation photons line but to follow the activity using the PHA mode, taking the reading immediately from the digital read-out on the analyzer every one minute. The count rates could then be corrected for the background due to ^{116m}In gamma rays.

The time behaviour of the decay of ^{112g}In is shown in fig. 4.8. The isomeric ratio for ^{112}In and the standard deviation were calculated as described previously. The experiment was repeated at another two neutron energies 13·49 ± 0·16 and 14·92 ± 0·16 MeV. The results are given in table II.2, each value of the isomeric ratio is the average of two measurements made at each neutron energy.

The results of this work with the values of other authors are shown in fig. 4.9, the isomeric ratio $\frac{\sigma_m}{\sigma_g}$ = 4·97 at 14·7 MeV measured by Rotzer[40] as well as the value 4·16 obtained by Minetti and Pasquarelli[13] also at 14·7 MeV are consistent with this work. The present values differ considerably from the single measurement of 13·3 at a neutron energy 14·0 MeV published by Curzio and Sona[11], however since these authors appear to have obtained a value of 10·8 m for $T_{½}g$ this difference is not surprising. Some measurements by Decowski et al[41] disagree with the present work, these workers calculated the two states separately and their errors are rather large.

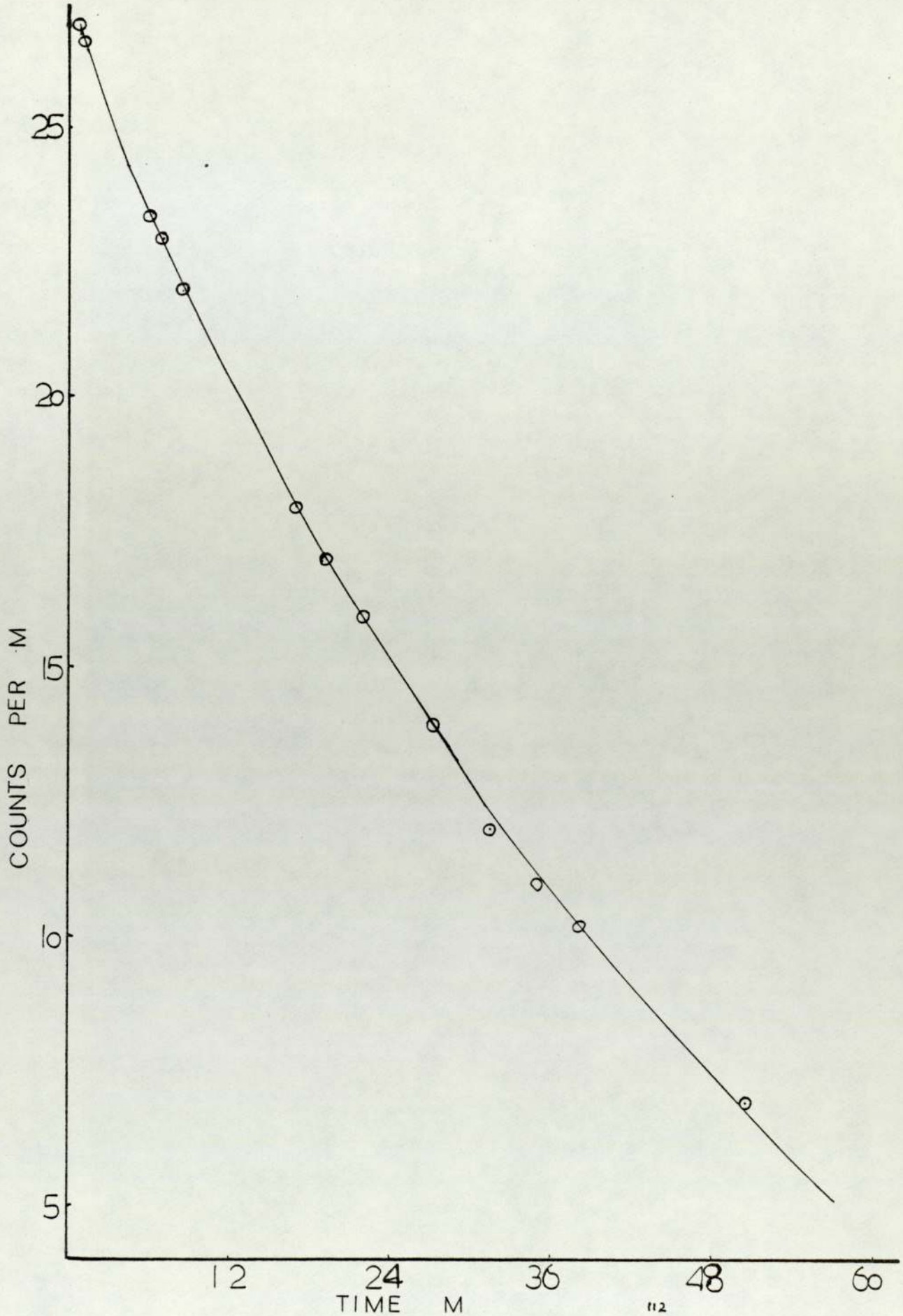

Fig(4.8) time behaviour of decay of In^{112}

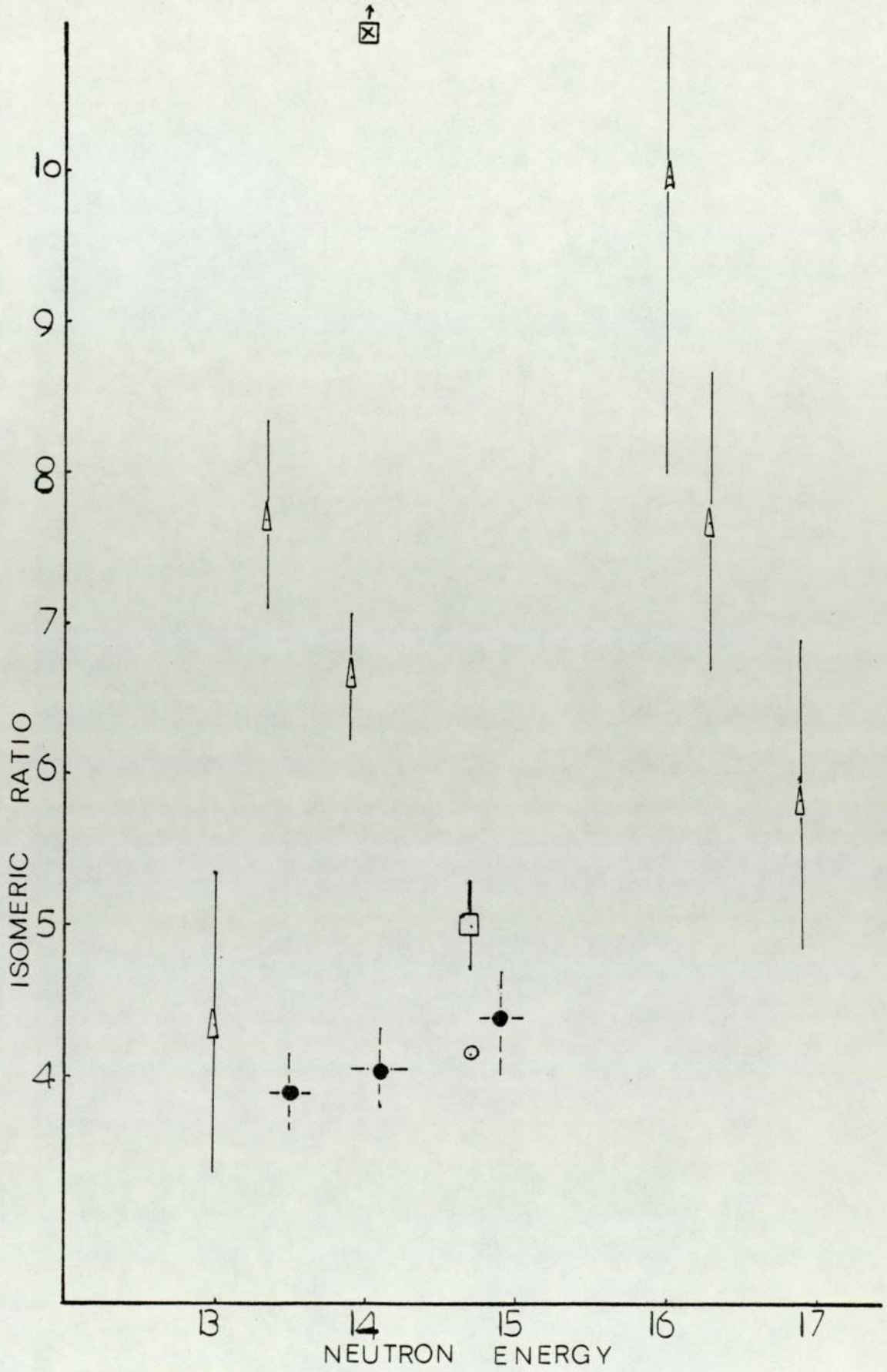

Fig(4.9) isomeric cross section ratio of $^{113}In(n,2n)^{112}In$ with values of other workers

• present work, □ ref(40), ⊖ ref(13), △ ref(41), ⊠ ref(11)

Table II.2

Neutron energy MeV	Number of experiments	Isomeric cross-section ratio
13·49 ± 0·16	2	3·90 ± 0·26
14·14 ± 0·2	2	4·05 ± 0·25
14·92 ± 0·16	2	4·42 ± 0·4

Results for the reaction $^{113}In(n,2n)^{112}In$

4.3.3 $^{198}Pt(n,2n)^{197m,g}Pt$ reaction

A sample of a few grams of natural platinum was bombarded for four hours in a similar arrangement to that described in the scandium measurements. Natural platinum consists of ^{190}Pt 0·013%, ^{192}Pt 0·78%, ^{194}Pt 32·9%, ^{195}Pt 33·8%, ^{196}Pt 25·2% and ^{198}Pt 7·19%.

The sample was surrounded with cadmium. Without the cadmium sheet one would expect about 300 times more activity from the fast neutron reaction, $^{198}Pt(n,2n)^{197}Pt$, than from the thermal neutron reaction, $^{196}Pt(n,\gamma)^{197}Pt$. This is small but not insignificant, therefore cadmium was used.

A spectrum taken at the end of irradiation is shown in fig. 4.10. This spectrum shows a large peak at about 77 KeV. In addition to the .077 MeV gamma ray from the decay of ^{197g}Pt this peak contains:

1) X-rays emitted with an energy of 0·074 MeV the characteristic radiation of ^{197}Au arising from internal conversion occurring after the ^{197g}Pt has emitted a β^- particle.

2) With isomeric transitions X-rays are emitted with energies characteristic of ^{197}Pt.

3) 0·075 MeV γ rays from ^{199}Pt arising from the reaction $^{198}Pt(n,\gamma)^{199}Pt$.

4) X-rays arising from the passage of β particles through Pt.

There was a peak in the spectrum at about 350 KeV, this is due to 0·346 MeV γ ray arising from the isomeric decay of ^{197}Pt, but also contains a contribution from the 0·328 MeV γ ray arising from the decay of ^{194}Ir and

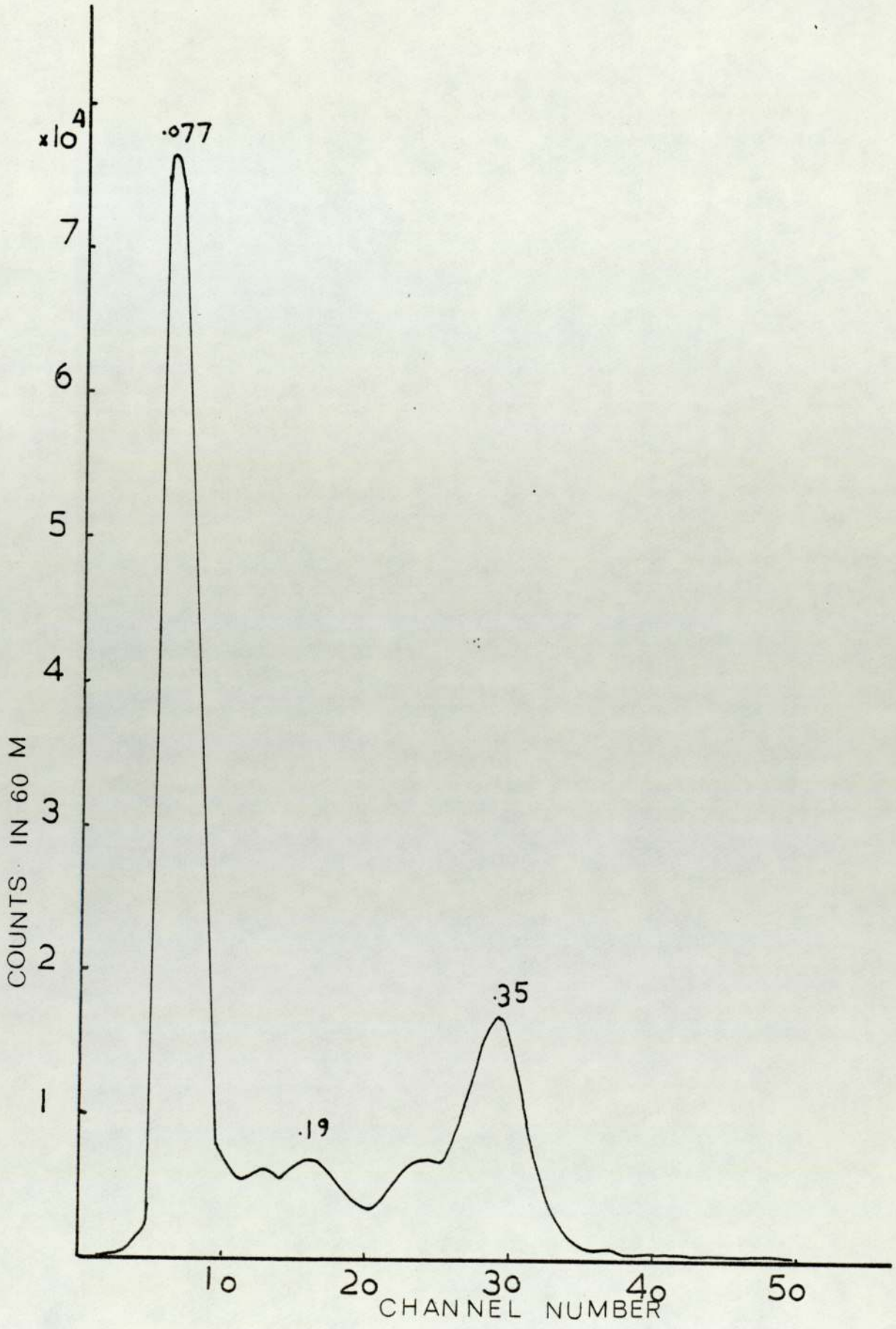

Fig (4.1o) γ rays spectra of ^{197}Pt

produced by the reaction $^{194}Pt(n,p)^{194}In$.

The intensity of the 0·19 MeV ray arising from ground state decay was very weak and it would be difficult to estimate with good accuracy. Thus the application of the method of measuring the isomeric cross-section ratio described in Chapter III of this thesis would be very difficult. It was decided therefore to attempt to estimate the isomeric cross-section ratio by applying the method of observing the decay of the isomeric and ground states respectively.

Samples were irradiated for four hours at angles of 0, 30 and 90 degrees to the incident beam, the energies of the neutrons at these angles were 15·37 ± 0·01, 15·2 ± 0·06 and 14·14 ± 0·1 MeV respectively.

The spectrum for ^{197}Pt immediately after irradiation using the NaI(Tl) well detector is shown in fig. 4·11 and the area under the peak of the metastable state, 0·346 MeV, was calculated. This is proportional to the activity A_{m2} of the metastable state at any time, t_1 after irradiation,

$$A_{m2} = \sigma_m N \emptyset \, e^{-\lambda m t_1}(1-e^{-\lambda m T}) \qquad \text{IV.3.1}$$

the symbols used are explained in Chapter III.
Equation IV.3.1 can be written in the form

$$A_{m2} = A_{m_1} \, e^{-\lambda m t_1} \qquad \text{IV.3.2}$$

where A_{m_1} is the activity of the isomeric state at the end of irradiation. Using the value of A_{m2} and equation IV.3.2, A_{m_1} was calculated.

As the isomeric ratio for ^{197}Pt was determined by comparing the relative intensities of two peaks at different energies, the area of the peak as recorded is

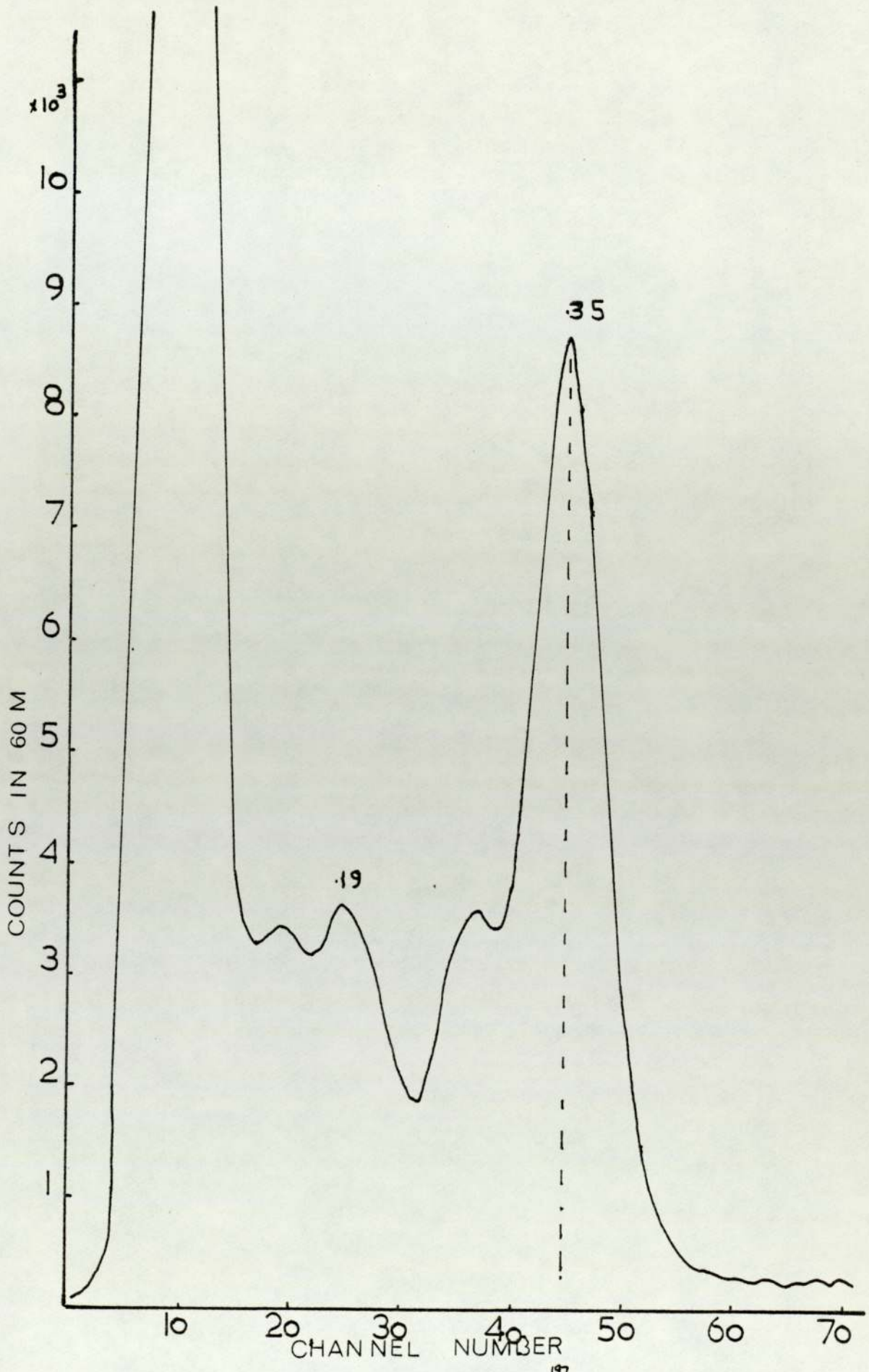

Fig (4.11) γ rays spectra of ^{197}Pt

not an absolute measure of the activity of the source since:

1) The disintegrations that take place do not all result in the emission of γ ray at 346 KeV. According to the decay scheme, fig. 4.2, only 97%[35] of the total do this, the chance that the gamma ray in fact will be emitted is denoted by the factor a.

2) Internal conversion is responsible for the fact that all the γ ray arising from decay do not appear as such in the count rate from platinum. The coefficient α is employed to denote the quotient of the number of conversion electrons emitted, by the actual number of γ ray emitted by a nuclide. When internal conversion takes place electrons in all the shells are involved, so that the coefficient α is the sum of α_K, α_L, and so on. With the aid of α the correction factor is determined that will indicate which part of the original gamma ray is left over

$$C = \frac{1}{1 + \alpha}$$

$\alpha_k = 3{\cdot}9 \pm 0{\cdot}4$ and K/L[33] $= 1{\cdot}8 \pm 0{\cdot}2$

Internal conversion at low energies is of high consequence, the estimated error was about ± 10%.

3) The symbol ζ is employed to denote the detection efficiency which is governed by the following conditions:

a. The geometry of the combination of detector and source.

b. The energy of the γ ray.

c. The type of scintillator used.

The factor ζ represents the ratio of the number of pulses in the output signal from the detector to the

number of γ rays emitted by the source. ζ was tabulated by Synder[42] for various sizes of crystals available including the size used for various γ ray energies.

4) The peak was produced not only by γ rays which transfer their energy by direct absorption as a result of photoelectric effect. Also involved are γ rays which are absorbed by the crystal by way of a sequence of events such as Compton scattering followed by absorption of the scattered quantum by photoelectric effect. The ratio of the number of pulses actually responsible for the peak, to the total number of pulses recorded is known as peak-to-total ratio p, it was taken from Synder[43] with ± 3% error.

5) It now remains only to determine the amount of absorption of the rays before they reach the crystal. For source emits more than one energy and is also of thickness X, the different energies will be absorbed by different amounts within the source itself, so that the fraction of photons of certain energy will depend on the thickness of the source. Correction for this, f_s, can be made with the following formula

$$f_s = \frac{1 - e^{\mu x}}{\mu x}$$

which gives the ratio of the number of photons of any one energy emitted from the end of the source to those which would be emitted if there were no self absorption. μ is the linear absorption coefficient in cm^{-1} if x is in cm. The coefficient used in the calculation of f_s was taken from Evans[44].

The activity A of a reaction product, present at

any time, resulting in a count rate A' in one of its characteristic γ photopeaks, is calculated using the relation

$$A = A'/aC\gamma Pf_s \qquad \text{IV.3.3}$$

The counting error was ± 1·4%.

The spectrum at about 18 hours after irradiation is shown in fig. 4.11, the peak at 0·35 MeV was due to ^{194}Ir which has a 19 hour half-life. From this the value of A_{m_1} was corrected for the activity of ^{194}Ir at the end of irradiation. The area under the peak of the ground state, 0·19 MeV, was calculated , the Compton background being subtracted: this area is proportional to the activity of the ground state, A_{g_2}.

A_{g_2} at any time, t_2, after irradiation, is given by

$$A_{g_2} = A_{g_1} e^{-\lambda g t_2} + A_{m_1} \frac{\lambda g}{\lambda g - \lambda m}(e^{-\lambda m t_2} - e^{-\lambda g t_2}) \qquad \text{IV.3.4}$$

A_{g_1} is the activity of the ground state at the end of irradiation. Using equation IV.3.4, the values of A_{g_2} and A_{m_1}, A_{g_1} can be calculated. Similar corrections to these described before have to be applied to A_{g_2} and the isomeric ratio can be calculated using the equation

$$\frac{A_{m_1}}{A_{g_1}} = \frac{\frac{\sigma m}{\sigma g}(1 - e^{-\lambda m T})}{\left(\frac{\sigma m}{\sigma g}+1\right)(1-e^{-\lambda g T}) + \frac{\lambda g}{\lambda g - \lambda m}\left[e^{-\lambda g T} - e^{-\lambda m T}\right]} \cdot \frac{\sigma m}{\sigma g}$$

IV.3.5

Results of the isomeric cross-section ratio for ^{197}Pt are shown in table II.3, with other workers in fig. 4.12.

The isomeric ratios measured were based on different conversion coefficients for the 192 KeV transition so the reported isomeric ratio values differed from one another due to the high uncertainty of this factor.

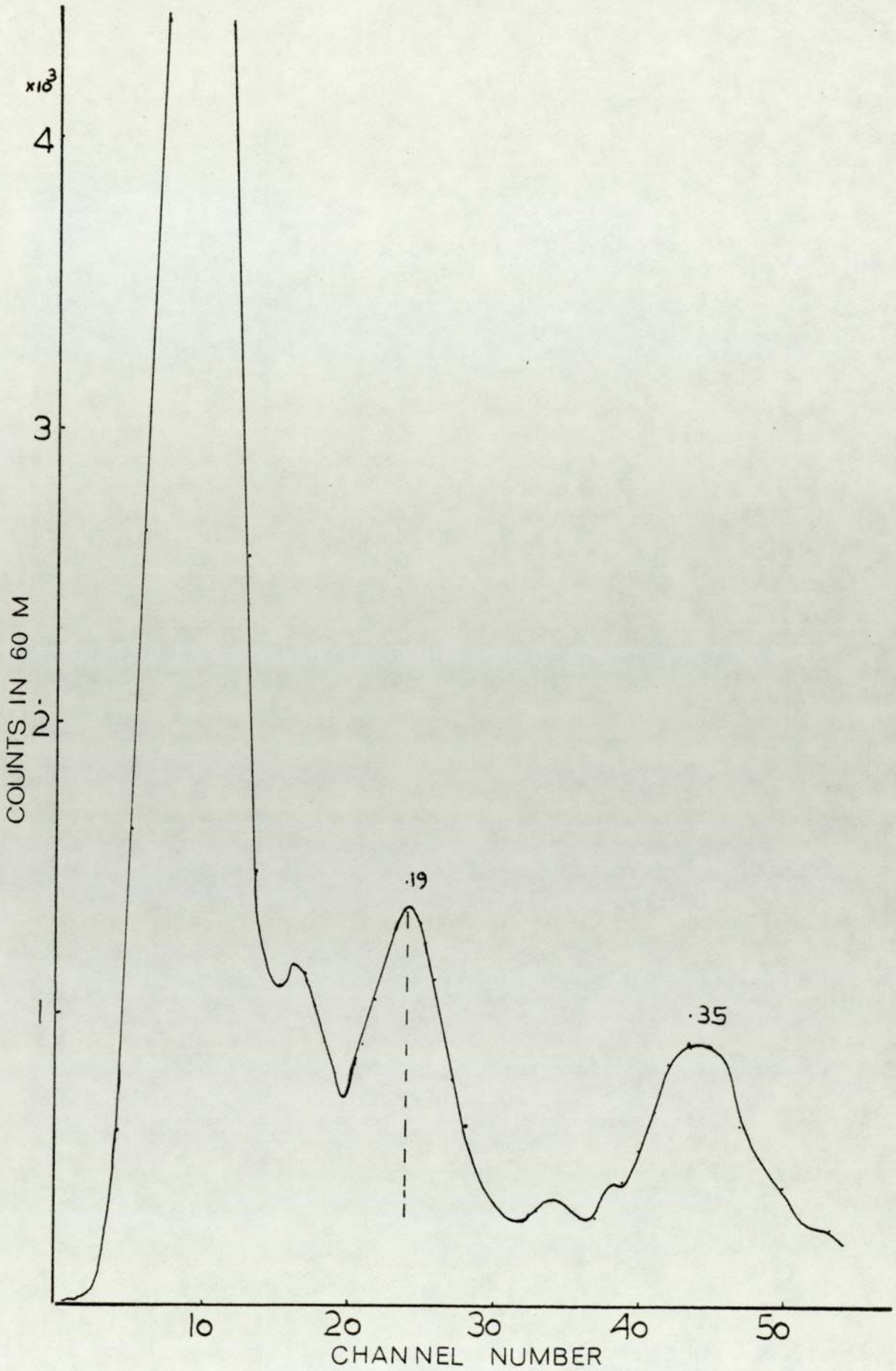

Fig (4.11) γ-ray spectra of ^{197}Pt

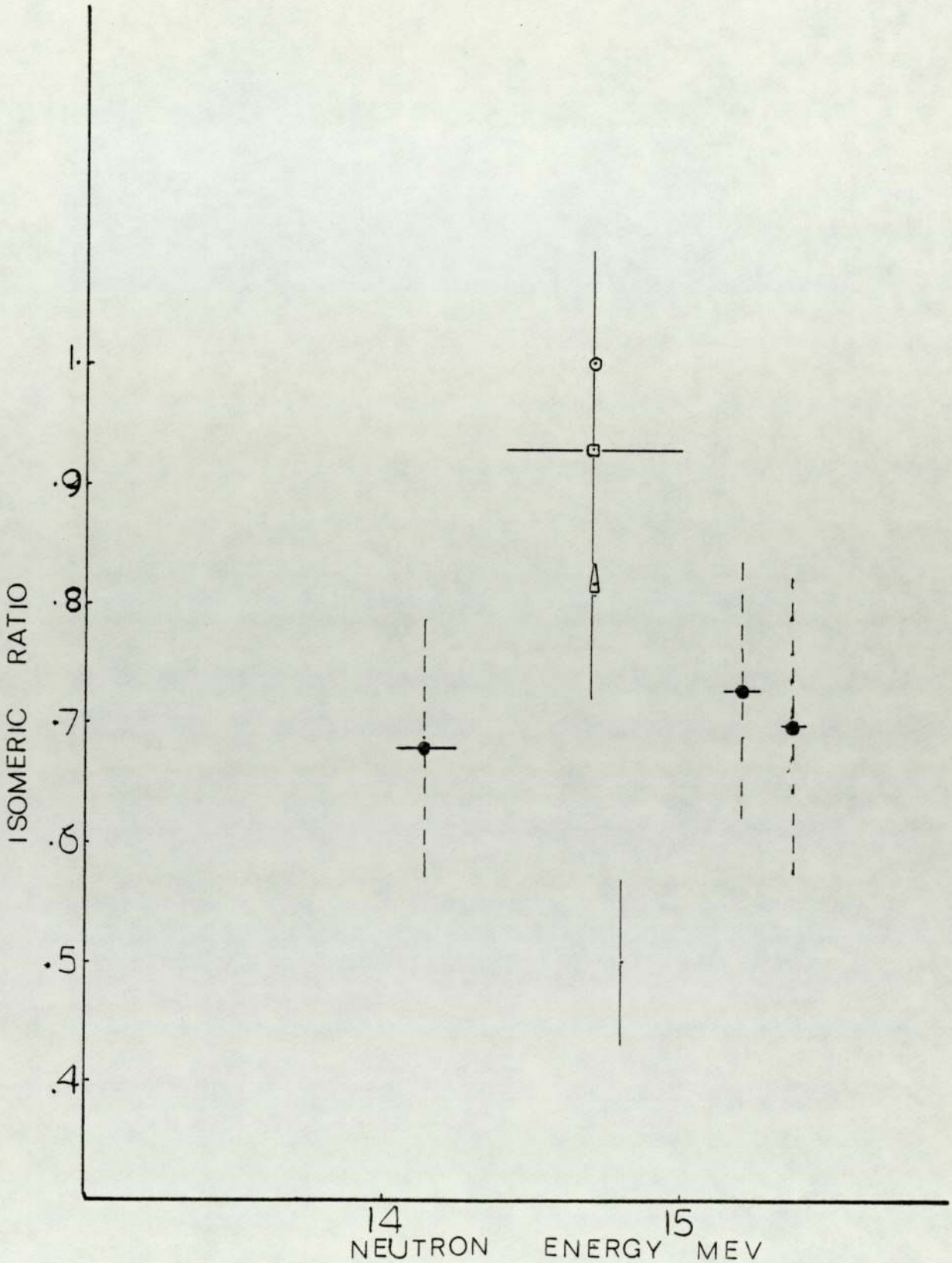

Fig (4.12) isomeric cross section ratio of $^{198}Pt(n,2n)^{197}Pt$ .. present work, ○ ref (45), □ ref (7), ▲ ref (8), . ref (9)

Table II.3

Neutron energy MeV	Isomeric ratio
14·14 ± 0·1	0·68 ± 0·11
15·2 ± 0·06	0·73 ± 0·15
15·37 ± 0·01	0.70 ± 0·11

Results for the reaction $^{198}Pt(n,2n)^{197}Pt$

IV.3.4 $^{76}Ge(n,2n)^{75m.g}Ge$ reaction

Natural germanium consists of ^{70}Ge 20·55%, ^{72}Ge 27·37%, ^{73}Ge 7·67%. ^{74}Ge 36·74% and ^{76}Ge 7·67%. A sample of natural germanium oxide in powder form, enclosed in a plastic tube, was used in the first experiment carried out on germanium. The sample was surrounded with cadmium sheet during irradiation to avoid as far as possible the production of $^{75m.g}Ge$ by the $^{74}Ge(n,\gamma)^{75}Ge$ reaction produced by thermal neutrons. Even without the cadmium sheet one would expect about 90 times more ^{75}Ge activity from the fast neutron reaction than from the thermal. The rapid transfer system was adapted to transfer the sample to the NaI(Tl) detector. The spectrum observed in the display for this sample is shown in fig. 4.13. The strong 511 KeV gamma ray shown may be attributed to ^{15}O (half-life 124s) produced by the (n,2n) reaction on ^{16}O.

To avoid the production of ^{15}O from ^{16}O germanium metal was used in the second experiment, the spectrum obtained is shown in fig. 4.14, the peak at 0·265 MeV due to the γ ray resulting from the decay of the ground state of ^{75}Ge is seen. However there was a little interference from ^{77}Ge, (11.3 h) which results in the peaks at 0·43, 0·56, 0·63. 0·73 and 0·8 MeV.

Because ^{75m}Ge has a short half-life the multiscale mode was used, the channel width and the base line were adjusted to include the photopeak, the adjustment was done by using standard sources of known γ ray energy.

Another experiment was carried on Ge with an irradiation time of 5 minutes, the 0·265 MeV γ ray

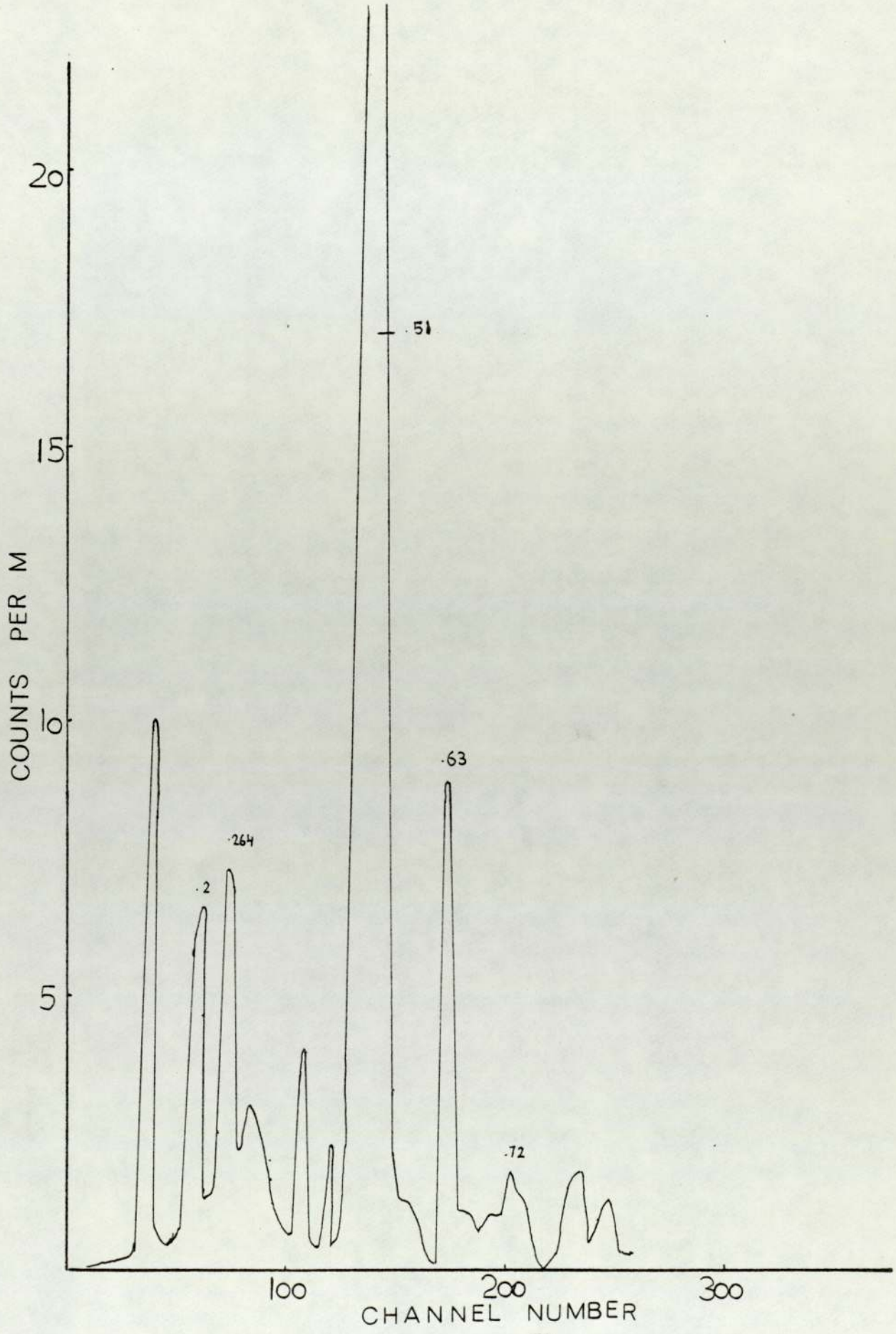

Fig(4.13) τ rays spectra of ^{75}Ge

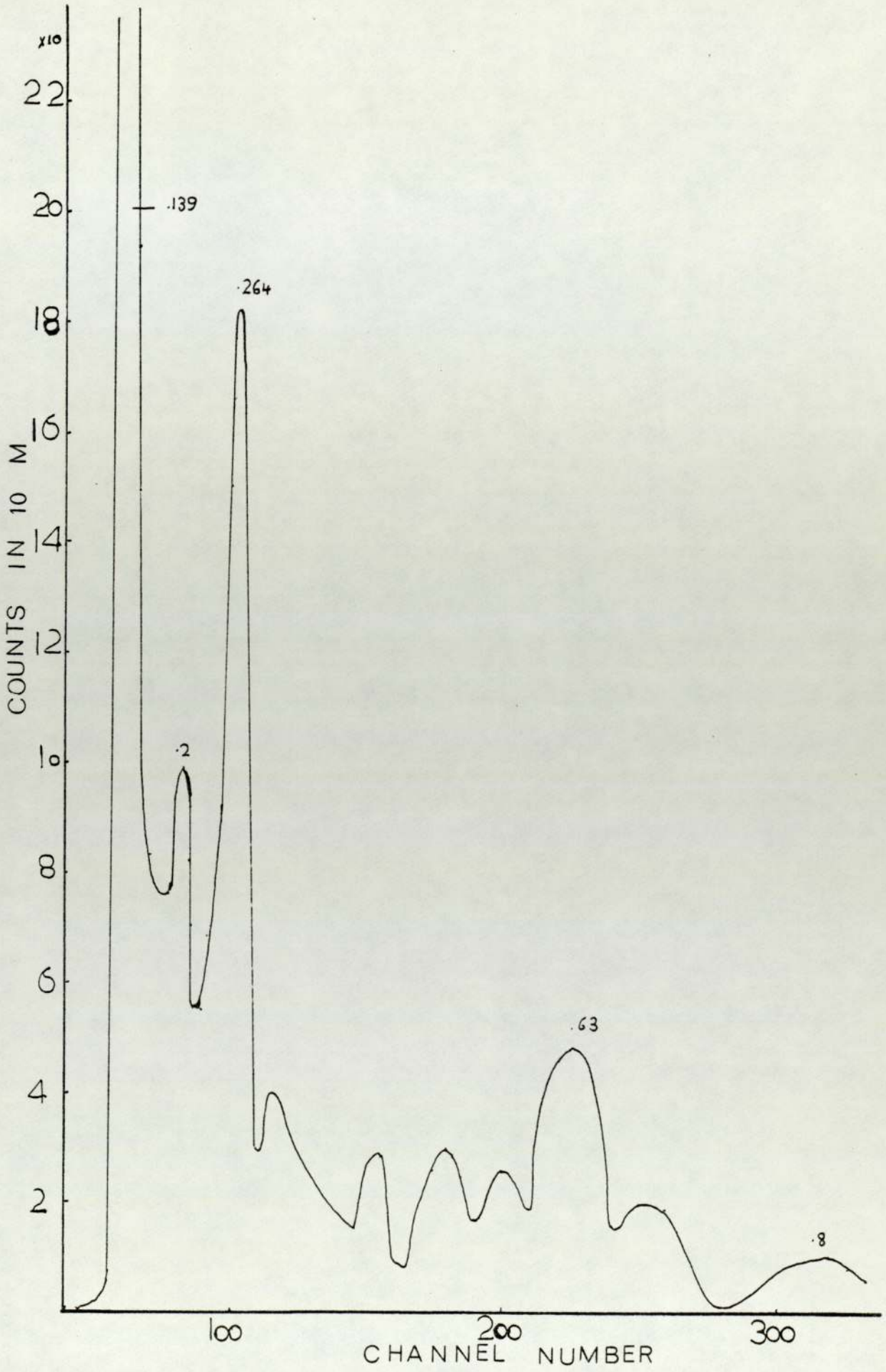

Fig(4.14) γ rays spectra of ^{75}Ge

was followed on the multiscale mode with a dwell time of 10 s using the well detector. The decay curve is shown in fig. 4.15.

It will be seen that although on the original spectrum there is clearly activity due to both the ground state and the isomeric state, the decay of the 0·265 MeV γ rays from the ground state does not depart significantly from that expected from a simple decay with the half-life of the ground state. This is because the large difference in half-lives of the isomeric and ground states means that the decay of the upper state does not contribute significantly to the ground state activity. This could be avoided with very short irradiation but the overall count rates would then be low.

This shows that the method of following the ground state decay is not ideally suited to situations where the ground state half-life is much longer than that of the upper state. Study of ^{75}Ge was therefore discontinued.

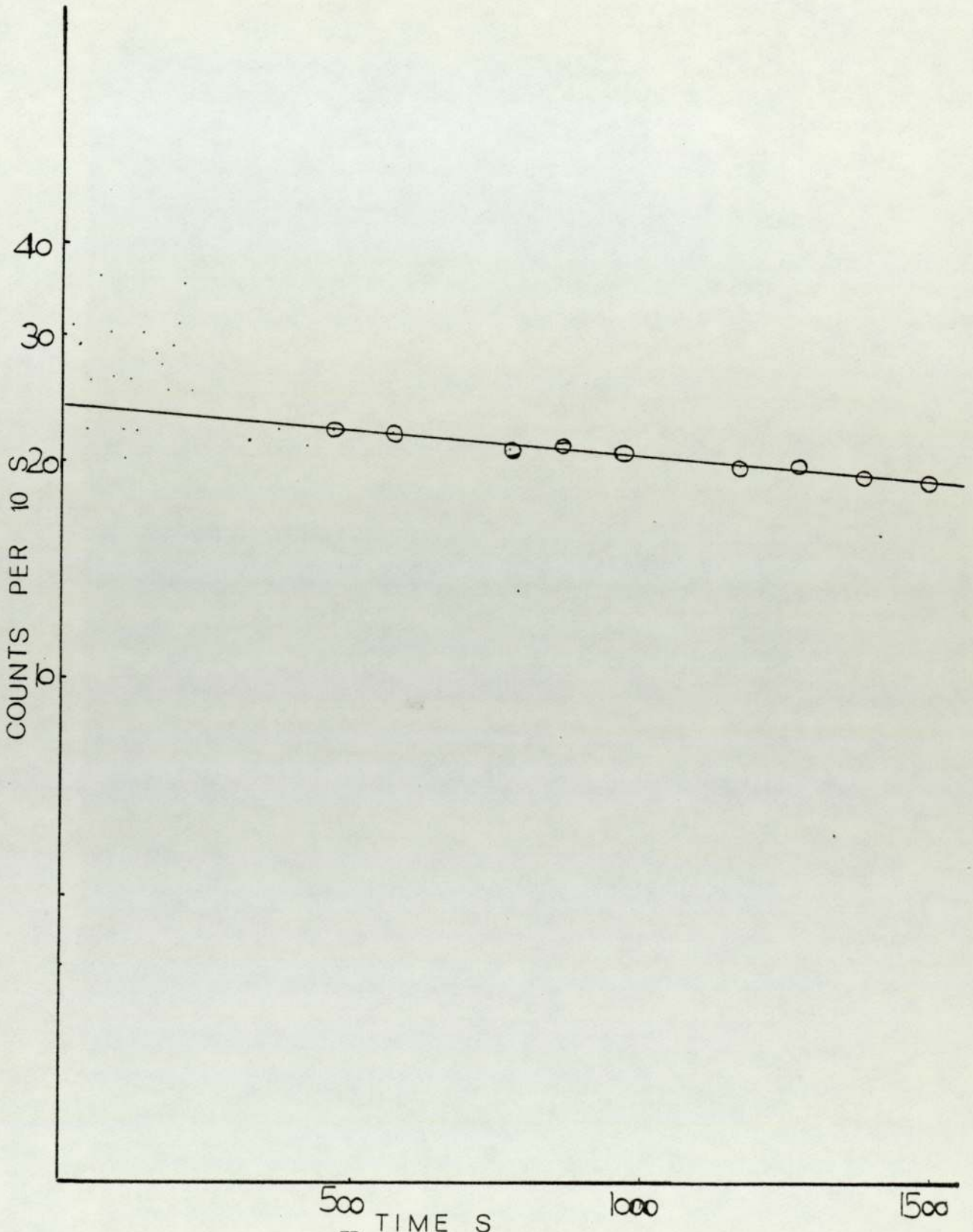

Fig (4.15) ^{75}Ge decay curve

CHAPTER V

THE THEORETICAL CALCULATION OF ISOMERIC CROSS-SECTION RATIOS

The formation of isomeric nuclei requires the use of nuclear reactions and in order to analyse these reactions some theory is required.

V.1 Statistics and nuclear reactions

There are two models for the nuclear reactions, the direct interaction model and the compound nucleus model. In the direct interaction model the incident particle interacts with a nucleon and not with the target nucleus as a whole. In the compound nucleus model, instead of the immediate emission of a particle after the initial interaction of the projectile, both the projectile and the particle can remain inside the nucleus, giving rise to new interactions, and the projectile energy is gradually shared with the target nucleus as a whole. When finally the energy, momentum and angular momentum only characterize the system and the memory of the mode of initial formation has been lost we are dealing with the compound nucleus of Bohr[46]. A classical system exhibiting an analogy to the compound nucleus is a heated liquid drop from which particles evaporate. In this case the emission is governed by the statistical characteristics of the system, the temperature which determines the shape of the energy spectrum and the average energy of emission. At 14 MeV it is unclear which of these two models is the better, however the compound nucleus approach seems to work well. In particular it may be appropriate for

(n,2n) reactions, and it will be used in this chapter.

V.2 Formation cross-section for compound nucleus

The probability of formation of the compound nucleus depends on the ease with which the projectile can enter the target nucleus, this involves the charge, energy of the projectile and the height of the potential barrier of the target nucleus. These factors are included in a function $T_l(E)$ called the barrier penetration coefficient. When the projectile has entered the nucleus, the distribution of angular momentum in the resulting compound nucleus will be governed by the spin of the target nucleus, the angular momentum of the projectile, and the multiplicity giving the total number of channels available in the compound nucleus. Vandenbosch and Huizenger[47] give an equation for the distribution of angular momentum in the compound nucleus and this is produced below:

$$\sigma(J_c) = \pi\lambda^2 \sum_{S=|I-s|}^{I+s} \sum_{l=|J_c-S|}^{J_c+S} \frac{(2J_c+1)}{(2s+1)(2I+1)} \overline{T_l(E)} \qquad \text{V.2.1}$$

In equation V.2.1 J_c is the angular momentum in the compound nucleus, E is the excitation energy, λ is the de Broglie wave length of the incoming particle divided by 2π, I is the spin of the target nucleus, s is the spin of the projectile and S is the combination of I and s called the channel spin.

V.3 The decay of the compound nucleus

The general expression[48] for the cross-section leading to emission of particle X is given by

$$\sigma(a,X) = \sigma_c \frac{F(x)}{\sum_i Fi} \qquad V.3.1$$

where σ_c is the cross-section for the formation of a compound nucleus, F(x) is proportional to the sum of the partial widths for the emission of particle X, summed over all possible final states of the residual nucleus, and $\sum_i Fi$ is summed overall modes of disintegration of the compound nucleus.

The relative probability $P_{J_c \rightarrow J_f}$ of a compound nucleus with spin J_c emitting a particle leading to a final state of spin J_f will depend on the density of levels with spin J_f and on the angular momentum taken by the particle.

If the probability of de-excitation by a particle of orbital angular momentum ℓ is taken[47] to be proportional to its transmission coefficient, then

$$P_{J_c \rightarrow J_f} \propto \rho(J_f) \sum_{S=|J_c-s|}^{J_c+s} \sum_{\ell=|J_f-S|}^{J_f+S} T_\ell(E) \qquad V.3.2$$

where $T_\ell(E)$ is the barrier transmission coefficient which refers to the emission of a particle from the compound nucleus, and $\rho(J_f)$ is the density of levels with spin J_f which is predicted theoretically[49,50] to be of the form

$$\rho(J_f) = \rho(o)\ (2J_f+1)\ \exp\left[-(J_f+\tfrac{1}{2})^2/2\sigma^2\right] \qquad V.3.3$$

In equation V.3.3 σ is the spin cut-off[51] parameter characterizing the distribution function, and $\rho(o)$ is the density of levels with spin zero which is taken to be[52] $e^{2\sqrt{Ea}}$, where E is the excitation of the final nucleus, and a is a parameter given by Blatt and

Weisskopf[48] which changes with the mass number of the final nucleus.

V.4 Calculation of the isomeric cross-section ratio

Using the method developed by Vandenbosch and Huizenga[47] it is possible to calculate the isomeric cross-section ratio, the calculation can be carried out in the following steps.

First the cross-section $\sigma(J_c)$ for forming a compound nucleus with spin J_c by absorption of a neutron of energy E is given by equation V.2.1. The total cross-section σ_{cpd} for the compound nucleus formation is then obtained by summation over the available J_c values.

The spin of the projectile s and target nucleus I can be taken from the table of isotopes, λ can be calculated from the relation $\lambda = \frac{\hbar}{p}$ where p is the momentum of the neutron and $\hbar$ is the Planck's constant divided by 2π. $T_\ell(E)$, the barrier penetration coefficient, for the neutron can be taken from the calculations of Feld et al.[53]

Next we must consider the decay of the compound nucleus by emission of two neutrons. It has been assumed[52] that the (n,2n) reaction cross-section is given by

$$\sigma(n,2n) = \sigma_{cpd} \frac{P(2n)}{\sum P(x)} \qquad V.4.1$$

where P(2n) is proportional to the probability of evaporating two neutrons from the compound nucleus, P(X) is the probability of evaporating any particle X, and $\sum P(x)$ is the total probability of decay of the compound nucleus, in (n,2n) reactions the competing reactions could be (n,n), (n,p) and (n,α).

Vandenbosch and Huizenga[47] give the cross-section for forming a spin state J_f in the final nucleus, $P(J_f)$, as

$$P(J_f) \propto \sigma(J_c)\, \rho(o)\, \frac{(2J_f+1)}{2\sigma^2} \exp\left[-(J_f+\tfrac{1}{2})^2/2\sigma^2\right] \sum_{S=|J_c-s|}^{J_c+S} \sum_{l=|J_f-S|}^{J_f+S} T_l(E) \qquad V.4.2$$

where $T_l(E)$ is now the barrier penetration coefficient for a particle X leaving the compound nucleus with excitation energy E, and s is the spin of the emitted particle x.

The total probability of forming a given final nucleus is found by summing over all the available J_f states.

The calculation for the cross-section with respect to the angular momentum in the final nucleus can be carried out for different values of the parameter σ .

It was assumed that the energy available to the particle to be evaporated is the excitation energy of the compound nucleus less the binding energy of the particle concerned. This will give the maximum energy available and only a few of the evaporated particles will receive this amount. In order to allow for this it was assumed that the distribution of energies available to all the evaporated particles was maxwellian and the average energy between zero and the maximum energy available was taken to be the most probable energy at the disposal of the evaporated particle. It is necessary to decide which of the two isomeric states the final angular momentum distribution will populate. To do this it is necessary to make some assumptions and

it has been assumed that the de-excitation of the final nucleus takes place by a gamma ray cascade and that dipole transitions are the most probable.

Consider the two isomeric levels with spin quantum numbers as shown in fig. V.1. State A will be populated directly by the angular momentum states, 0, 1, and 2: similarly state B will be populated by 5, 6, and 7. The contribution from the angular momentum states 3 and 4 is assumed to be shared by both A and B.

The population of the states is taken to be directly proportional to the formation cross-section. Hence by means of the considerations given above the populations of the two levels can be found if the isomeric spin states were known. It is then assumed that the ratio of the populations give the isomeric cross-section ratios. To obtain the best fit of the calculated cross-section ratio to the measured ones the value σ should be varied, this allows an estimate to the spin cut-off parameter σ to be obtained.

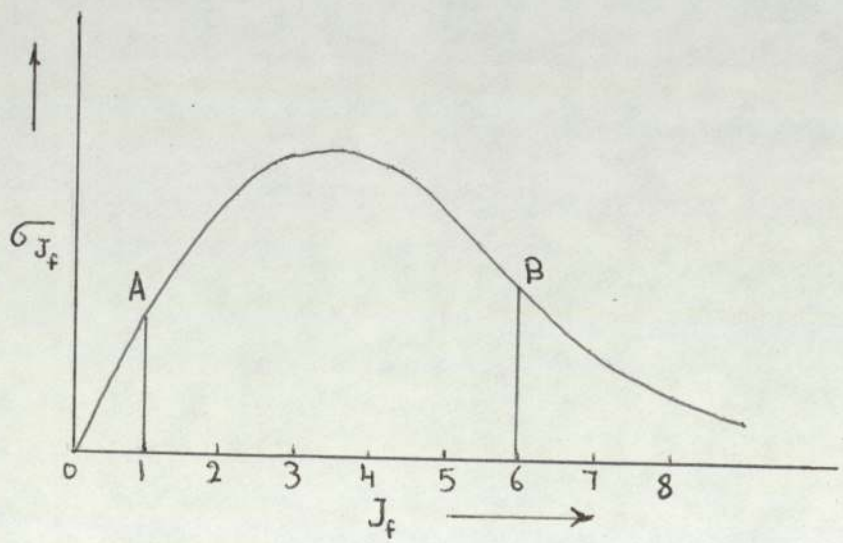

Fig V.1 Population of spin states

CHAPTER VI

CONCLUSIONS

The method used in this work for measuring the isomeric cross-section ratio takes advantage of the fact that members of an isomeric pair are genetically related in that the ground state is populated both directly by the (n,2n) reaction and by isomeric transition from the metastable state. Applying the method of least squares to the time behaviour of the decay of the ground state the isomeric cross-section ratio was determined.

The results so obtained are independent of several sensitive factors such as photopeak detection efficiency, exact knowledge of the decay scheme of the ground state, absorption corrections and sample uniformity. These factors invariably constitute the major portion of uncertainty in the results of earlier experiments.

Therefore the present work should have good reliability.

For very short half-lives the rapid transfer system was used to transfer the sample in a few seconds to the detector.

For the isomers pairs under consideration, two possible situations appear in regard to their decay schemes. The first type is that in which the metastable state is longer lived than the ground state, the scandium and indium isomeric pairs are of this type. The remaining isomeric pairs germanium and platinum are of the second type in which the metastable state is shorter lived than the ground state.

This method does work and give good results with the necessary resolution and with the benefits of the present day sophistication of counting equipment.

The following factors impose certain limits on the applicability of this method.

1. The isomeric pairs must be genetically related in that the ground state is populated both by direct reaction and by isomeric transition from the metastable state.

2. The half-lives must not be too different.

3. The sample must be strong enough in the sense that the disintegration rate is high, so that if there is a very short-lived activity making it necessary to make several counts in a short time interval in order to follow the time behaviour of the decay. Then these counts should not have too high a statistical error.

Using the Huizenga-Vandenbosch method, described in Chapter V, Section V.3, it is possible to calculate the isomeric cross-section ratio. Comparing the data obtained theoretically with the measured values, valuable information about the excited final nucleus arising from the nuclear reaction can be obtained, in particular a determination of the probable value of the spin cut-off parameter, σ , and the moment of inertia of the nucleus deduced.

Other fast neutron reactions to which the method might be applied are $^{198}Au(n,2n)^{197}Au$, $^{144}Sm(n,2n)^{143}Sm$, $^{82}Se(n,2n)^{81}Se$, and $^{191}Ir(n,2n)^{190}Ir$. The method is not of course restricted to fast neutron reactions, it could be applied to the measurement of isomeric cross-section ratios in any type of reaction.

APPENDIX I

Computer programme for calculting the isomeric ratio.

```
10    Select print 015
20    Dim U(50), R(50), A(50), B(50), C(50), D(50), E(50),
      F(50), G(50), H(50), I(50)
30    Read M, N, T
40    Data 0·002947, 0·00019727, 180
50    A = 0:  B = 0:  C = 0:  D = 0:  E = 0:  F = 0:  G = 0:
      H = 0:  I = 0
60    Print M, N, T
70    A = 0:  B = 0:  C = 0:  D = 0:  E = 0:  F = 0:  G = 0:
      H = 0:  I = 0
80    For S = 1  to 30
90    Read U(s), R(s)
100   Data 20, 3866, ....
110   Print U(s), R(s)
120   A(s)=( M.(1-exp(-N.T)).(exp(-N.U(s) )))/(M-N)
130   B(s)=(N.(1-exp(-M.T)).(exp(-M.U(s) )))/(M-N)
140   C(s)=(A(s)-B(s) )
150   D(s)=((1-exp(-M.T)).(exp(-M.U(s))))
160   A  =  A + A(s)
170   B  =  B + B(s)
180   C  =  C + C(s)
190   D  =  D + D(s)
195   Print C(s), D(s)
200   E  =  E + (C(s) ↑ 2)
210   F  =  F + (C(s). D(s) )
220   G  =  G + (D(s) ↑ 2)
230   H  =  H + (C(s) · R(s) )
```

APPENDIX I (contd)

```
240   I = I + (D(s).R(s))
250   Next S
260   X = ((H.G) - (I.F))/((F.G) - (F↑2))
270   Y = ((E.I) - (F.H))/((E.G) - (F↑2))
280   Print x,y
290   Z = (x/y)
300   Print Z
310   Stop
```

APPENDIX II

Second programme for calculating the standard deviation in the isomeric cross-section ratio.

```
10    Select print 015
20    Dim R(40), C(40), D(40), A(40), B(40), E(40),
      F(40), G(40), H(40), I(40), J(40)
30    Read x, y, N
40    Data ...
50    A = 0:  B = 0:  E = 0:  F = 0:  G = 0:  H = 0:  I = 0:
      J = 0
60    Print x, y, N
70    A = 0:  B = 0:  E = 0:  F = 0:  G = 0:  H = 0:  I = 0:
      J = 0
80    For s = 1 to 37
90    Read R(s), C(s), D(s)
100   Data ...
110
120
130
140   A(s) = (x. C(s))
150   B(s) = (y. D(s))
160   E(s) = (A(s) + B(s))
170   F(s) = (R(s) - E(s))
180   A  = A + A(s)
190   B  = B + B(s)
200   E  = E + E(s)
210   F  = F + F(s)
220   G  = G + (F(s) ↑ 2)
230   H  = H + (C(s) ↑ 2)
```

APPENDIX II (contd)

```
240   I  =  I + (C(s)·D(S))
250   J  =  J + (D(s)↑2)
260   Next S
270   K = sq((G.J)/(N.((H.J) - (I↑2))))
280   L = sq((H.G)/(N.((H.J) - (I↑2))))
290   Print k, L
300   Z = ((k/x) + (L/y))
310   Print Z
320   Stop
```

REFERENCES

1. Nuclear Physics - An Introduction by Burcham, W.E., (1963).
2. Modern Trends in Activation Analysis. (1969), Volume 2.
3. J. Brgosko, P. Decowski, K. Siwek-Diament and A.Wiethelmi, Nucl. Phys., 74, (1965), 438.
4. J.R. Huizenga and R.V. Vandenbosch, Phys. Rev., 120, (1960), 1305.
5. A.J. Cox and P.E. Francois, J. Inorg. Nucl.Chem., 31, (1969), 2957.
6. S.M. Qaim, J. Inorg. Nucl. Chem., 32, (1970), 1789.
7. S.M. Qaim, Nucl. Phys., A 185, (1972), 614.
8. P. Winiwarter, Nucl. Phys., A 158, (1970), 77.
9. S.K. Mangal andC.S. Khurana, Nucl. Phys., 69, (1965), 158.
10. Shoji Okumura, Nuc. Phys., A 93, (1967), 74.
11. G. Curzio and P. Sona, Nuova Cimento 54B, (1968), 319.
12. R. Prasad and D.C. Sarkar, Nucl. Phys., A 94, (1967), 476.
13. B. Mineiti and A. Pasquarelli, Z. Physik, 217, (1968), 83.
14. S.K. Mangol and P.S. Gill, Nucl. Phys., 49, (1963), 510.
15. P.K. Eapen and G.N. Salaita, J. Inorg. Nucl. Chem., 37, (1975), 1121.
16. T.H. Kao and W.L.Alford, Nucl. Phys., A 237, (1975), 11.
17. Activation analysis with neutron generators, Norgol Walla, Sam S. 1973.

18. Dr. D. Crumpton. Thesis. (1957).

19. P. Thoneman, J. Moffat, O. Roaf and J. Sanders, Proc. Phys. Soc. (London), 61, (1948), 483.

20. Principles of Activation Analysis. Paul Kruger (1971).

21. J.L. Fowler and J.E. Brolley, Rev. Mod. Phys., 28, 103, (1956).

22. E.A. Burrill, Neutron production and protection. (1963).

23. Introduction to nuclear physics. Harold A. Enge.

24. Advances in activation analysis, J.M.A.Lenihan, S.J. Thomson and V.P. Guinn, (1972).

25. K. Brondi, R. Engelmann, V. Hepp, E. Kluge, H. Krehbiel, and U. Mayer-Burkhout, Nucl. Phys., 59, (1964), 33.

26. J.H. Bjerregarrd, P.F. Dahl, O. Hansen, and G. Sidenius, Nucl. Phys., 51, (1964), 641.

27. Modern radiochemical practice by Cook and Duncan.

28. Errors of observations and their treatment by J. Topping.

29. Hermann Weigmann, Z. Physik, 167, (1962), 549.

30. S.B. Burson, W.C. Jordan, and J.M. Le Blanc, Phys. Rev., 96, (1954), 1555.

31. J.Z. Ruan, Y. Yoshizama, and Y. Koh, Nucl. Phys., 36, (1962), 431.

32. E. Bleuler, J.W. Blue, S.A.Chowdary, A.C. Johnson, and D.J. Tendam, Phys. Rev., 90, (1953), 464.

33. A.J. Hanafield, H.T. Easterday, and J.M. Hollander, Nucl. Phys., 64, (1965), 379.

34. Paresh Mukherjee, Nucl. Phys., 64, (1965), 65.

35. C.M. Lenderer, J.M. Hollander, and I. Perlman, Table of isotopes. Sixth edition (1967).

36. L.A. Rayburn, Proc. Phys. Soc., 77, (1961), 508.

37. J. Karolyi, J. Csikai and G. Peto, Nucl. Phys., A 122, (1968), 234.

38. R.J. Prestwood and B.P. Bayhurst, Phys. Rev., 121, (1961), 1438.

39. P.E. Francois, Analyst, 93, (1968), 720.

40. Rotzer, H., Nucl. Phys., 109, (1968), 694.

41. P. Decowski, W. Grochulski, J. Karoli, A. Marcinkowski, J. Piotrowski, E. Saad, and Z.Wilhelmi, Nucl. Phys., A 204, (1973), 121.

42. B.J. Synder, Nucl. Inst. and Meth., 53, (1967), 313.

43. B.J. Synder and G.F. Knoll, Nucl. Inst. and Meth., 40, (1966), 261.

44. C.M. Davisson and R.D. Evans, Rev. Mod. Phys., 24, (1952), 79.

45. M. Bormann, H.H. Bissem, E. Magiera, and R. Warnemunde, Nucl. Phys., A 157, (1970), 481.

46. N. Bohr, Nature, 137, (1936), 344.

47. R. Vandenbosch and J.R. Huizenga, Phys. Rev., 120, (1961), 1313.

48. Theoretical Nuclear Physics, Blatt and Weisskopf, (1952).

49. H.A. Bethe, Rev. Mod. Phys., 9, (1937), 84.

50. C. Bloch, Phys. Rev., 93, (1954), 1094.

51. Torleif Ericson, Nucl. Phys., 11, (1959), 481.

52. D. Crumpton, A.J. Cox, P.N. Cooper, P.E. Francois, and S.E. Hunt, Inorg. Nucl. Chem., 31, (1969), 1.

53. B.T. Feld, H. Feshbach, M.L. Goldberger, M. Goldstein, and V.F. Weisskopf, AEC Report NYO - 636, (1951).